Relationships among Intermodel Spread and Biases in Tropical Atlantic Sea Surface Temperatures

ELSA MOHINO

Department of Physics of the Earth and Astrophysics, Universidad Complutense de Madrid, Madrid, Spain

BELÉN RODRÍGUEZ-FONSECA

Department of Physics of the Earth and Astrophysics, Universidad Complutense de Madrid, and Instituto de Geociencias, Madrid, Spain

C. ROBERTO MECHOSO

Department of Atmospheric and Oceanic Sciences, University of California, Los Angeles, Los Angeles, California

TERESA LOSADA

Department of Physics of the Earth and Astrophysics, Universidad Complutense de Madrid, Madrid, Spain

IRENE POLO

Department of Physics of the Earth and Astrophysics, Universidad Complutense de Madrid, Madrid, Spain, and Department of Meteorology, University of Reading, Reading, United Kingdom

(Manuscript received 12 December 2018, in final form 22 March 2019)

ABSTRACT

State-of-the-art general circulation models show important systematic errors in their simulation of sea surface temperatures (SST), especially in the tropical Atlantic. In this work the spread in the simulation of climatological SST in the tropical Atlantic by 24 CMIP5 models is examined, and its relationship with the mean systematic biases in the region is explored. The modes of intermodel variability are estimated by applying principal component (PC) analysis to the SSTs in the region 70°W–20°E, 20°S–20°N. The intermodel variability is approximately explained by the first three modes. The first mode is related to warmer SSTs in the basin, shows worldwide connections with same-signed loads over most of the tropics, and is connected with lower low cloud cover over the eastern parts of the subtropical oceans. The second mode is restricted to the Atlantic, where it shows negative and positive loads to the north and south of the equator, respectively, and is connected to a too weak Atlantic meridional overturning circulation (AMOC). The third mode is related to the double intertropical convergence zone bias in the Pacific and to an interhemispheric asymmetry in the net radiation at the top of the atmosphere. The structure of the second mode is closer to the mean bias than that of the others in the tropical Atlantic, suggesting that model difficulties with the AMOC contribute to the regional biases.

1. Introduction

State-of-the-art general circulation models (GCMs) of the coupled atmosphere–ocean system show important systematic errors (biases) in their simulation of the present climate. The present paper focuses on the tropical Atlantic Ocean, where biases in annual mean sea surface temperature (SST) are large (Fig. 1a). In particular, along the equator biases can be of such magnitude (Flato et al. 2013) that the sign of the simulated SST zonal gradient along the equator is opposite to the observations (Richter and Xie 2008; Davey et al. 2002; Richter et al. 2014; Zuidema et al. 2016). The GCMs also struggle with the observed SST variability in the tropical Atlantic (Richter et al. 2014), in particular

Supplemental information related to this paper is available at the Journals Online website: https://doi.org/10.1175/JCLI-D-18-0846.s1.

Corresponding author: Elsa Mohino, emohino@ucm.es

DOI: 10.1175/JCLI-D-18-0846.1

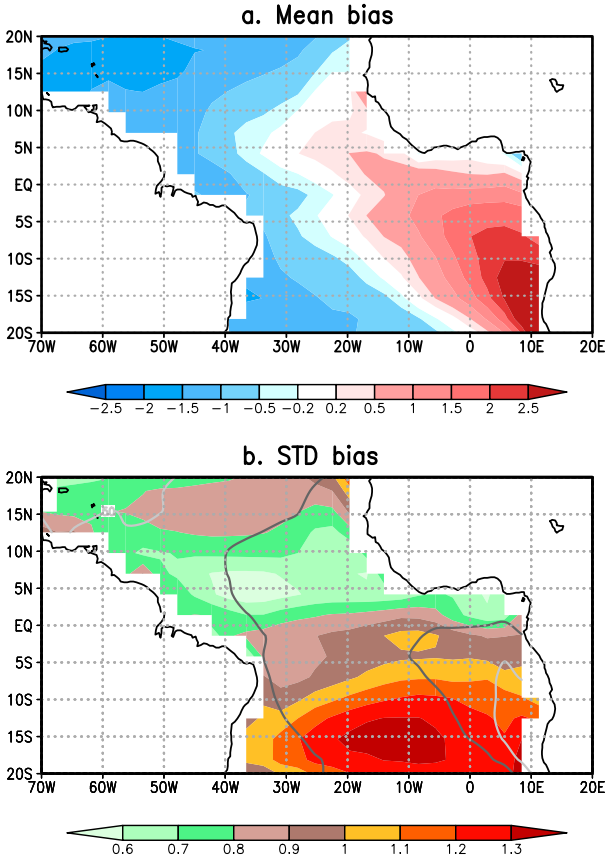

FIG. 1. SST bias and its intermodel variability in the tropical Atlantic: (a) average of SST bias using the 24 models (K) and (b) standard deviation of SST bias among the 24 models (K). Dark (light) gray contours mark regions where the standard deviation is above 100% (50%) of the averaged SST bias.

its main mode of variability, the Atlantic Niño (I. Polo et al. 2018, unpublished manuscript). Mean SST biases hinder the operation of key dynamical feedbacks in the region and lead to overestimation of the stochastic component of the local SST variance (Ding et al. 2015; Nnamchi et al. 2015; Dippe et al. 2018). In addition, as SST anomalies in the tropical Atlantic can impact the tropical Pacific climate through alterations of the Walker circulation (Rodriguez-Fonseca et al. 2009), biases in the former region can impact the model's representation of climate variability in the latter region. In particular, the tropical Atlantic biases have been shown to weaken and shift eastward the local simulated main ascending motions that result from the recent observed tropical Atlantic warming trend, leading to an underrepresentation of the strengthening of the Pacific trade winds observed in recent decades (McGregor et al. 2018; Kajtar et al. 2018). SST biases such as those described above reduce our confidence in the predictions and projections by current GCMs for the tropical Atlantic basin and adjacent regions.

The simulation of tropical rainfall by CGCMs also has particularly pervasive biases, which result in a too symmetric structure across the equator. This double intertropical convergence zone (ITCZ) bias (Mechoso et al. 1995) remains a feature of concern in current GCMs (Bellucci et al. 2010; Li and Xie 2014; Oueslati and Bellon 2015; Xiang et al. 2017). The models also have difficulties with the simulation of low marine cloud cover, which is especially important in the southeastern tropical Pacific and Atlantic Oceans and in the Southern Ocean (Karlsson et al. 2008; Lin et al. 2014; Mechoso et al. 2016). The effect on the total albedo of such underestimation of low cloud cover tends to be erroneously compensated by an overestimation of cloud albedo, especially over the southeastern tropical Atlantic (Engström et al. 2014). Consistently with the rainfall biases, the models also show errors in their simulation of upper-tropospheric clouds in the tropics (Jiang et al. 2012). Outside the tropics, GCM simulations tend to capture a too weak Atlantic meridional overturning circulation (AMOC; Danabasoglu et al. 2014; Wang et al. 2014), a feature that is at least partially due to a too salty and warm South Atlantic Antarctic intermediate water through its impact on the AMOC return flow (Zhu et al. 2018). Moreover, the sea ice thickness and extent produced by GCMs are too small compared to observations, especially around Antarctica where simulations show very large spread (Turner et al. 2013; Shu et al. 2015).

Many studies have addressed the causes for the tropical Atlantic SST biases. The underrepresentation of the low-level stratocumulus deck over the southeastern tropical Atlantic has been mentioned as one of the potential causes of the local SST warm bias through an excessive shortwave radiative flux into the ocean (Ma et al. 1996; Huang et al. 2007; Hu et al. 2008; Toniazzo and Woolnough 2014; Voldoire et al. 2014). Hourdin et al. (2015) find that the overestimation of near-surface humidity by the atmospheric component of GCMs could provide a comparable contribution to the warm bias through a too low evaporative cooling. Other studies emphasize the westerly wind bias at the surface over the equatorial Atlantic, which results in a simulated thermocline that is too shallow in the west and too deep in the east (Richter and Xie 2008; Xu et al. 2014; Richter 2015; Goubanova et al. 2019; Shi et al. 2018), inhibiting the development of the equatorial cold tongue (Richter et al. 2012; Voldoire et al. 2014). The resulting equatorial warm SST bias can be advected eastward along the equator and southward along the African coast through propagating oceanic downwelling Kelvin waves, contributing to further warming of the southeastern tropical Atlantic (Toniazzo and Woolnough 2014; Goubanova

et al. 2019). The existence of the westerly wind bias and associated errors in wind stress in the simulations can be a consequence of several factors, such as the underrepresentation of zonal momentum flux across the top of the boundary layer (Zermeño-Diaz and Zhang 2013) and/or excessive (deficient) rainfall over equatorial Africa (South America) with insufficient lower-tropospheric diabatic heating over the Amazon (Zermeño-Diaz and Zhang 2013; Richter et al. 2012). The simulation of spurious barrier layers in the southeastern equatorial Atlantic could also hinder the development of the cold tongue, contributing to the local warm SST bias (Breugem et al. 2008). Song et al. (2015) suggest that the warm bias over the eastern equatorial Atlantic and the southeastern tropical Atlantic could have a strong contribution from errors in the simulation of ocean dynamics and mixing processes. Models also show a too weak Benguela Current and too strong Angola Current, the combination of which would result in too much heat being transported into the southeastern tropical Atlantic where SSTs become too high (Xu et al. 2014; Koseki et al. 2018). Although the ultimate reasons for the tropical Atlantic SST biases might be model dependent, the positive feedbacks between wind stress, clouds, and SSTs seem to be key for maintaining and even enhancing the biases (Toniazzo and Woolnough 2014).

The global extent of GCM biases has also led to the formulation of hypotheses on the relationship among remote biases. Zhang et al. (2014) suggested that the warm bias in the southeastern tropical Pacific is related to a cold SST bias in the tropical North Atlantic through a weakening of a Hadley circulation from the latter to the former. Sasaki et al. (2014) showed that the removal of the equatorial Atlantic SST bias leads to an improvement in the representation of the tropical Pacific climatology. Cabos et al. (2017) argued that failures in the representation of the South Atlantic Anticyclone south of 20°S were important contributors to the warm bias in the tropical Atlantic. Hwang and Frierson (2013) argued that cloud biases in the Southern Ocean could be accountable for a large part of the "double ITCZ" bias. The too weak cloud cover in the region results in increased shortwave energy flux into the ocean leading to local warming. This, in turn, shifts the simulated raising branch of the Hadley cell and the ITCZ too far south due to altered interhemispheric energy fluxes (Kang et al. 2008; Li and Xie 2014). Mechoso et al. (2016) showed that this remote link is stronger in models with a strong sensitivity to the stratocumulus–SST feedback. Wang et al. (2014) connected SST biases worldwide to a too weak simulation of the AMOC. They suggested that the too warm SSTs in the southeastern Pacific and Atlantic can be related to the too weak simulated AMOC through an interhemispheric connection with the cold biases in the monsoon areas of West Africa, India, and Asia.

Different approaches have been followed in investigations of the causes for GCM biases. One approach is based on examining the time evolution of errors in simulations initialized with observations (e.g., Huang et al. 2007; Toniazzo and Woolnought 2014; Voldoire et al. 2014). Another approach has been based on performing sensitivity experiments with models in which the atmosphere–ocean coupling is only allowed in selected regions (Cabos et al. 2017). However, one of the most common approaches to shed light on the underlying physical processes at work for the biases is to take advantage of a multimodel framework and contrast the simulations with different models and parameterizations. Such contrast is typically performed in a region by averaging the variable of interest in a box and comparing it with other averaged variables in the region (Bellucci et al. 2010; Zermeño-Diaz and Zhang 2013; Hwang and Frierson 2013; Xu et al. 2014; Zhang et al. 2014; Oueslati and Bellon 2015; Hourdin et al. 2015). Other works take this same approach but with a wider focus, seeking to compare the simulated pattern of the variable in a wider domain (Wang et al. 2014; Li and Xie 2014). This is the approach taken in this manuscript to contrast the simulation of SSTs in the whole tropical Atlantic. In this region, models tend to show higher agreement among their SST biases north of the equator, around 5°N, while the strongest disagreement is observed south of 5°S, where the intermodel standard deviation of SST biases is above 1°C (Fig. 1b). Such meridional gradient in the intermodel spread of SSTs contrasts with the more zonal SST gradient shown by the mean bias pattern (Fig. 1a). The maximum intermodel standard deviation is not collocated over the region of maximum mean systematic bias in the southeastern tropical Atlantic, but displaced to the west.

In the present paper, we seek to understand which are the processes dominating this intermodel variability (Fig. 1b) and if these same processes could be responsible for the mean biases (Fig. 1a). To this aim, we examine the spread in the simulation of annual mean SST in the tropical Atlantic (70°W–20°E; 20°S–20°N) by 24 models participating in phase 5 of the Coupled Model Intercomparison project (CMIP5; Taylor et al. 2012) and explore its relationship with the mean systematic biases in the region. We apply a principal component analysis to show that most of the variance in the representation of SSTs in the tropical Atlantic can be understood with the first three modes. We then evaluate the similarity of the spatial patterns associated with each of these modes with the mean bias pattern to assess the likelihood that a

TABLE 1. List of the models used in the study: number used in the study, model name, institution and country, and number of years used.

Model No.	Model name	Institution and country	Years used
1	ACCESS1.0	Commonwealth Scientific and Industrial Research Organization (CSIRO) and Bureau of Meteorology (BOM), Australia	500
2	BCC_CSM1.1	Beijing Climate Center (BCC), China Meteorological Administration, China	500
3	BNU-ESM	College of Global Change and Earth System Science (GCESS), Beijing Normal University (BNU), Beijing, China	559
4	CanESM2	Canadian Centre for Climate Modeling and Analysis (CCCma), Canada	996
5	CCSM4	National Center for Atmospheric Research (NCAR), United States	501
6	CESM1-CAM5	NSF–DOE NCAR, United States	319
7	CMCC-CMS	CMCC–Centro Euro-Mediterraneo per i Cambiamenti Climatici, Italy	500
8	CNRM-CM5	Centre National de Recherches Meteorologiques (CNRM), Météo-France and Centre Europeen de Recherches et de Formation Avancee en Calcul Scientifique (CERFACS), France	850
9	CSIRO Mk3.6.0	CSIRO, Marine and Atmospheric Research, Queensland Climate Change Centre of Excellence (QCCCE), Australia	500
10	FGOALS-g2	Institute of Atmospheric Physics (IAP), Chinese Academy of Sciences, Tsinghua University (THU), China	700
11	GFDL-ESM2G	NOAA GFDL, United States	500
12	GFDL-ESM2M	NOAA GFDL, United States	500
13	GISS-E2-H	NASA/Goddard Institute for Space Studies (GISS), United States	531
14	GISS-E2-R	NASA/GISS, United States	550
15	HadGEM2-CC	Met Office Hadley Centre, United Kingdom	240
16	HadGEM2-ES	Met Office Hadley Centre, United Kingdom	575
17	INM-CM4.0	Institute for Numerical Mathematics (INM), Russia	500
18	IPSL-CM5A-LR	Institut Pierre Simon Laplace (IPSL), France	1000
19	MIROC4h	Atmosphere and Ocean Research Institute (AORI), The University of Tokyo, National Institute for Environmental Studies (NIES), Japan Agency for Marine-Earth Science and Technology (JAMSTEC), Japan	100
20	MIROC5	AORI, NIES, JAMSTEC, Japan	670
21	MIROC-ESM-CHEM	JAMSTEC, AORI, NIES, Japan	255
22	MPI-ESM-LR	Max Planck Institute for Meteorology, Germany	1000
23	MRI-CGCM3	Meteorological Research Institute (MRI), Japan	500
24	NorESM1-M	Norwegian Climate Centre, Norway	501

certain mode could be more relevant than the others for exacerbating the pattern of mean SST bias in the tropical Atlantic. In section 2 we present the data and methods used. In section 3 we analyze the characteristics of the three main modes and relate them to the mean bias in tropical Atlantic SSTs. Finally, we discuss our results and present our main conclusions in sections 4 and 5.

2. Data and methods

a. Data

Our guiding criterion for selection of CMIP5 models used in this study was to have as many models as possible that provide access to most of the variables of direct interest to this work. Table 1 shows our final selection of models. Table 2 displays the output variables from which we compute annual mean climatologies. In selected cases, seasonal climatologies are used. To facilitate the comparison, all variables were interpolated to a T42 Gaussian grid (approximately 2.8° × 2.8° in longitude and latitude).

In addition to the direct output of the variables shown in Table 2, we also computed the following:

- Atlantic meridional overturning circulation, which is defined as

$$\Psi(\varphi, z) = \int_H^z \int_{\lambda_{\text{west}}}^{\lambda_{\text{east}}} v(\varphi, \lambda, \xi) R_T \cos\varphi \, d\lambda \, d\xi, \qquad (1)$$

where $v(\varphi, \lambda, \xi)$ is the meridional velocity of the ocean, R_T is Earth's radius, H is the sea bottom depth, ξ is the depth coordinate for the integration (positive downward), z is the depth coordinate for the AMOC, φ is latitude, and is λ longitude. To reduce the noise, a 9-point smoothing was applied twice to the values

TABLE 2. List of variables that were obtained as a direct output from the models, their abbreviations in the plots, and their dimensions and units.

Variable	Abbreviation	Dimensions	Units
Surface temperature	tso	lon × lat	K
Precipitation	pr	lon × lat	mm day^{-1}
Sea level pressure	psl	lon × lat	hPa
Zonal wind	u	lon × lat × pressure level	m s^{-1}
Meridional wind	v	lon × lat × pressure level	m s^{-1}
Total cloud fraction	clt	lon × lat	%
TOA outgoing longwave radiation	rlut	lon × lat	W m^{-2}
TOA outgoing shortwave radiation	rsut	lon × lat	W m^{-2}
TOA outgoing longwave flux assuming clear sky	rlutcs	lon × lat	W m^{-2}
TOA outgoing shortwave flux assuming clear sky	rsutcs	lon × lat	W m^{-2}
Surface upward latent heat flux	hfls	lon × lat	mm day^{-1}
Sea ice area fraction	sic	lon × lat	%
Sea water meridional velocity	vo	lon × lat × depth	m s^{-1}
Sea water salinity	so	lon × lat × depth	psu
Sea water potential temperature	thetao	lon × lat × depth	K

obtained for each model. The units of the AMOC are Sverdrups (1 Sv $\equiv 10^6\,\mathrm{m}^3\,\mathrm{s}^{-1}$).

- Ocean heat content (K) in the upper ocean, which is defined by

$$\mathrm{OHC300} = \frac{\int_{\mathrm{surf}}^{z=300\,\mathrm{m}} T\,d\xi}{300}, \tag{2}$$

where T is the potential temperature of the ocean.

- Total (shortwave plus longwave) outgoing radiation at the top of the atmosphere (W m^{-2}).
- Longwave and shortwave cloud radiative effects (W m^{-2}), which are defined as the difference between the outgoing longwave and shortwave radiation, respectively, at the top of the atmosphere at clear-sky conditions minus at all-sky conditions. Positive (negative) values indicate that the effect of clouds is to reduce (increase) longwave (shortwave) radiation loss to space; that is, they indicate a warming (cooling) effect of clouds. Clear-sky outgoing longwave radiation was not available for two of the 24 models (CMCC-CSM and GISS-E2-H), and clear-sky outgoing shortwave radiation was not available for the GISS-E2-H model.
- The local relationship between SST and cloud cover in the tropical South Atlantic, which for each model is estimated as the grid point temporal correlation at monthly time scale between SST and total cloud fraction. All months of all years are used for each model in the calculation.

We have selected the long CMIP5 preindustrial control simulations in order to cover as many years as possible without the influence of varying radiative forcings. Our conclusions are not dependent on this choice, as the analysis performed (see section 2b) yields the same modes of intermodel spread when calculated with the historical simulation (not shown).

The mean SST bias is calculated as the difference between the annual climatology averaged across the 24 models minus the observed annual climatology for 1870–2013. The latter corresponds to the HadISST1 database (Rayner et al. 2003). This is a reconstructed global gridded datasets based on ship measurements from the Met Office Marine Data Bank, and on satellite estimates from the mid-1980s onward.

Observed estimates of net outgoing total radiation at the top of the atmosphere and shortwave cloud radiative effect are obtained from edition 4.0 of the Clouds and the Earth's Radiant Energy System (CERES) EBAF-TOA dataset (Loeb et al. 2018). Three products from the Global Energy and Water Cycle Experiment (GEWEX) cloud assessment database (Stubenrauch et al. 2013) are used for the cloud fractional cover: climatological values of ISCCP (1984–2007), AIRS-LMD (2003–09), and TOVS Path-B (1987–94). Version 2.3 of the Global Precipitation Climatology Project (GPCP) monthly precipitation analysis (Adler et al. 2003) is used to calculate the precipitation climatology in the 1979–2017 period.

b. Methods

To analyze intermodel spread in the representation of climatological SSTs in the tropical Atlantic we apply

an intermodel empirical orthogonal function (EOF) analysis (von Storch and Zwiers 2003) to the annual mean output from the models in the region 70°W–20°E, 20°S–20°N. In preparation for the analysis, the data were weighted by the average area of the cell. The results are not sensitive to the actual choice of the meridional boundaries for the analysis, as very similar modes are obtained in the region 70°W–20°E, 30°S–30°N (not shown). To further evaluate the robustness of our results, we tested the EOFs obtained when focusing only on the spatial pattern of the bias, as in Hourdin et al. (2015). For this purpose, for each model separately we removed the mean SST value over the tropics (averaging between 20°S and 20°N) before EOF analysis. Such removal provides the same modes of intermodel spread (correlations between principal components above 0.74 in the first three modes). We note that application of the EOF analysis to the climatological annual means and the climatological biases yields the same result because the covariance matrix is not affected by addition or subtraction of a fixed field (i.e., the observed climatology). The principal components associated with each EOF are standardized, and the different variables are regressed onto them. In the reminder of the paper we will refer to these regressions as anomalies. To estimate the statistical significance of the patterns, a two-tailed Student's t test is used. The level of statistical significance is chosen as 0.05 throughout this study. All the correlations shown in the scatterplots throughout this paper are statistically significant at the selected level.

We are also interested on how the modes of intermodel spread are related to the annual mean bias in tropical Atlantic SST. To this end, we apply a multilinear analysis to fit the spatial pattern of the mean bias of the 24 models used in the study. The multilinear regression model is given by

$$y_i = \alpha x1_i + \beta x2_i + \gamma x3_i + \varepsilon_i, \tag{3}$$

where y_i refers to the SST bias at grid point i; $x1_i$, $x2_i$, and $x3_i$ are the values of the SST projected onto the PC associated with the first, second, and third mode of intermodel spread, respectively, at grid point i; and ε_i is the unfitted residual. The coefficients α, β, γ, and ε in Eq. (3) are obtained by least squares estimation. Note that the regression model used has no intercept.

3. Results

In the following, the results of our analysis are explained in terms of patterns associated with positive values of the PC. As the analysis is linear, those models that show negative values of the PC are related to an intermodel variability pattern opposite to the one described.

a. *The first mode of intermodel spread in tropical Atlantic SSTs*

The first mode in the EOF analysis of intermodel spread in tropical Atlantic SSTs shows a coherent pattern over the whole tropics of this basin with maximum loads in the central part south of the equator (Fig. 2a). The amplitude of the principal component (PC) indicates the models with stronger loading of this EOF (Fig. 2b). There is no apparent relationship between the amplitude of the PC and the horizontal resolution of the model in its original grid (not shown). The strongest value of the PC in Fig. 2b corresponds to the CSIRO Mk3.6.0 model, which has an overall cold bias in the tropical Atlantic (Gordon et al. 2010; Hourdin et al. 2015). Since this model appears as an outlier, we repeated the EOF analysis without it (i.e., using only 23 models). We obtained very similar results for the three leading EOFs, except for a switch in order between the second and third modes (not shown). For this reason, we decided not to delete any model from our set. In the remainder of the paper, therefore, it is understood that our conclusions for the second and third mode have to be interchanged if we had not included information from the CSIRO model.

Returning to the first mode in the EOF analysis of intermodel spread in tropical Atlantic SST biases, Fig. 2a shows positive anomalies over the tropical Pacific and Indian Oceans, peaking in the eastern part of the subtropical ocean gyres. Such a configuration of anomalies suggests warmer (colder) SSTs for those models with a positive (negative) PC (Fig. 2b). The first mode explains a great part of the intermodel variability of SST in the tropical Atlantic (64.6%), and is separated from the second mode according to North's rule of thumb (North et al. 1982). In addition, this first mode of intermodel spread in SST is highly insensitive to whether the region used to perform the EOF calculation is the whole tropics (20°S–20°N), the tropical Pacific east of the date line (180°–80°W, 20°S–20°N), or even if the midlatitudes are included (60°S and 60°N), with correlations between the original PCs (Fig. 2b) and those obtained for the different regions of 0.92, 0.85, and 0.60, respectively. This insensitivity suggests that the intermodel variability in SST described by the first mode, even though it is clearly present in the tropical Atlantic, is not restricted to this basin but rather is part of a global-scale pattern.

Rainfall anomalies in the tropics associated with the SST pattern in Fig. 2a evidence a southward shift of the ITCZ in the tropical Atlantic, eastern equatorial Pacific, and Indian basins (Fig. 2c). This shift is consistent with

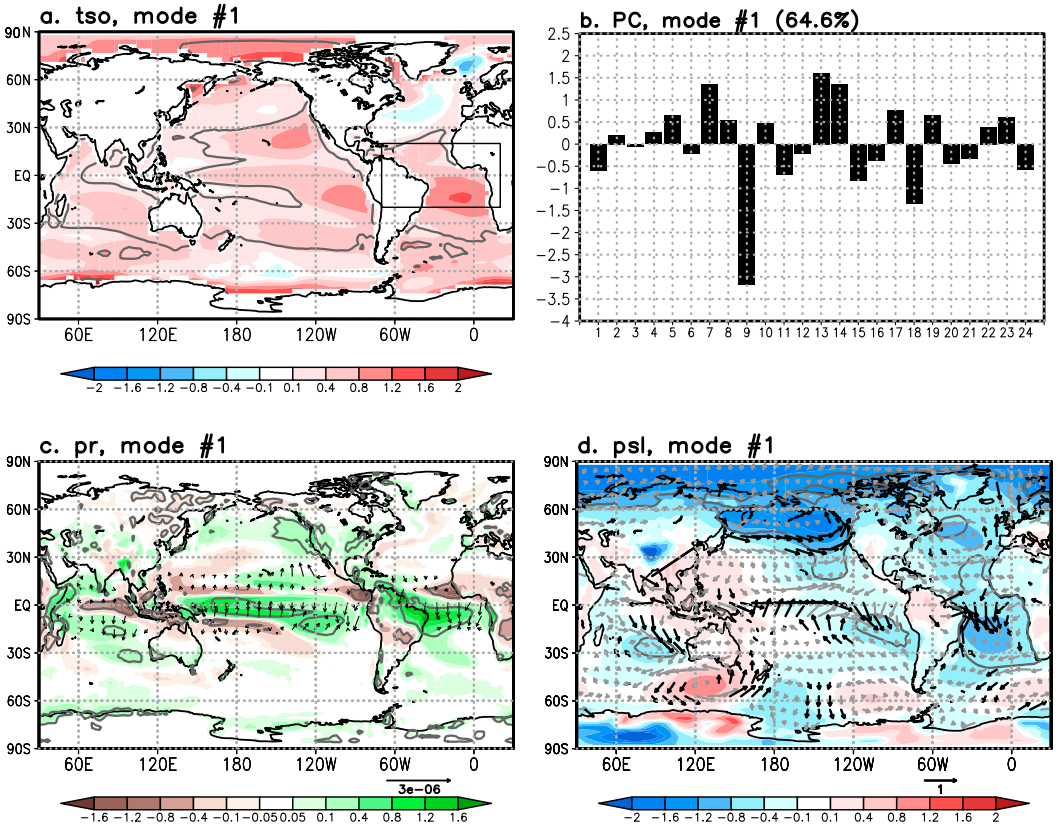

FIG. 2. First mode of intermodel variability in the tropical Atlantic. (a) Regression of surface temperature onto the first PC (K per standard deviation). Values over land are masked out. (b) Standardized PC (nondimensional) for each model. (c) Regression of rainfall onto the first PC (mm day^{-1} per standard deviation). (d) Regression of sea level pressure (shaded) and winds at 925 hPa (arrows) onto the first PC (hPa and m s^{-1} per standard deviation, respectively). Box in (a) shows the tropical Atlantic region where the EOF analysis is performed. Gray contours mark regions where the regression is statistically significant. Black arrows in (c) show the gradient in the SST in (a). Black arrows in (d) show regions where the regression of zonal or meridional wind is statistically significant.

the local southward anomalous gradient of SSTs and southward cross-equatorial surface anomalous winds (Fig. 2d) (Lindzen and Nigam 1987; Takatama et al. 2012; Diakhaté et al. 2018). In addition, the associated pattern of sea level pressure anomalies includes negative values in the subtropical South Atlantic, and the southeastern Pacific and Indian Oceans, where there are associated anomalous cyclonic surface circulations (Fig. 2d), which are consistent with the local warm SSTs.

To gain insight into the reasons for the existence of this dominant mode of intermodel SST spread we show in Fig. 3a the net radiative flux anomalies at the top of the atmosphere (shortwave plus longwave, positive out of the atmosphere) associated with the first PC. The consistency between the anomalies in SST and in net radiative flux, especially over the eastern part of the Atlantic, Pacific, and south Indian basins (Fig. 3a), suggests that the main contribution to the worldwide SST warm anomalies shown in Fig. 2a comes from a decreased loss in net radiation by the atmosphere. Such a warming affects the upper ocean, increasing its heat content in the tropics, especially in the southern and eastern parts of the basins (Fig. 3d). In the southeastern tropical Atlantic 16 out of the 24 models underestimate the net radiation flux loss to space (Fig. 4a). The models for which such underestimation is strong tend to show higher values of PC1 and stronger warm SST biases in the region (Figs. 4a,b). A mixed layer heat budget analysis further agrees with the notion that the main warming effect on the ocean surface is the increase in downward shortwave radiation (see section 1.1 in the online supplemental material). Conversely, the first mode does not show statistically significant associations with the mass transport in the Atlantic, as represented by the AMOC anomalies (Fig. 3b).

The decreased loss of net radiation in the eastern part of the tropical Atlantic, Pacific, and Indian basins takes place in regions characterized by large and persistent

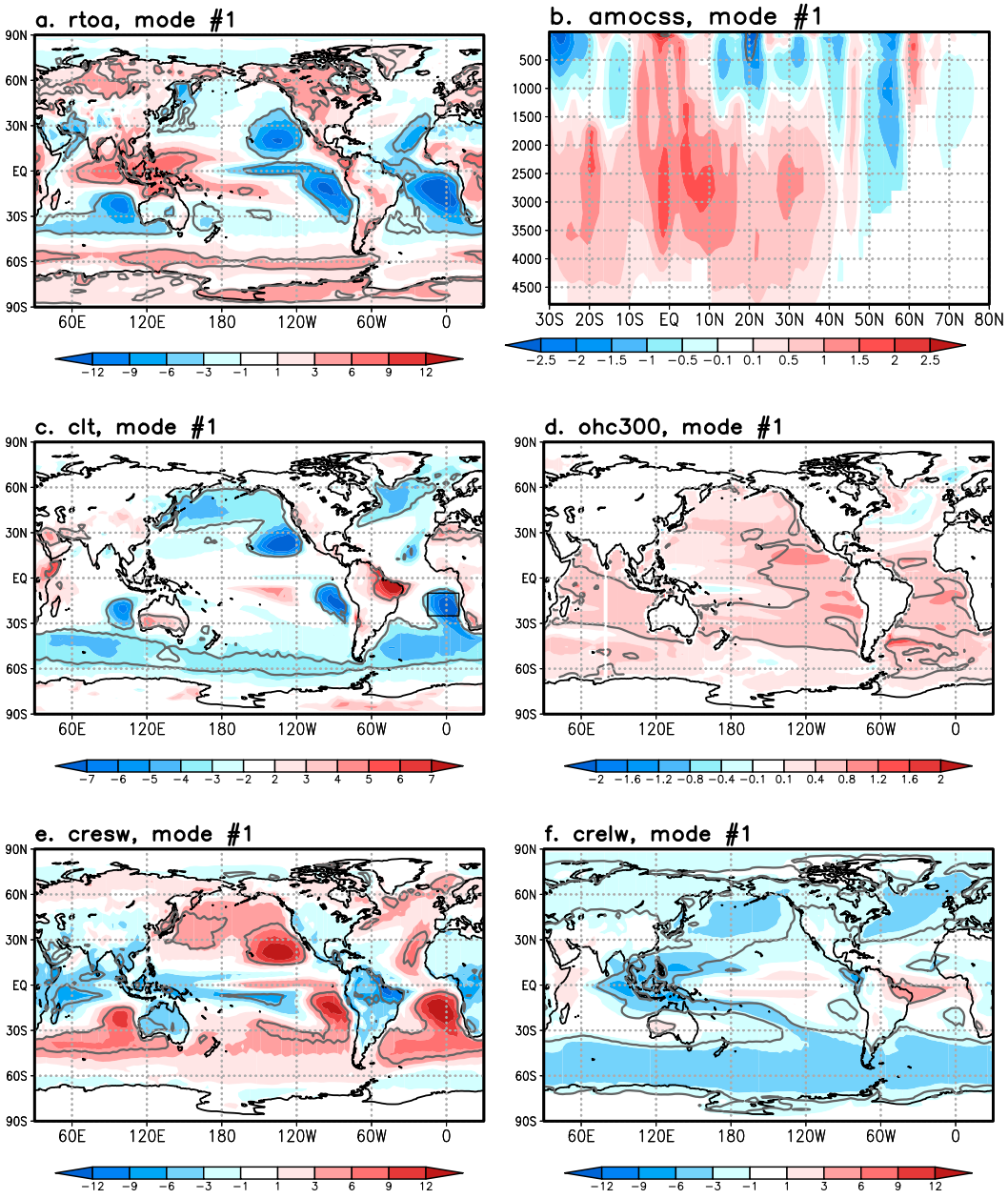

FIG. 3. Possible causes for the first mode of intermodel variability in the tropical Atlantic. (a) Regression of outgoing total radiation (longwave plus shortwave) at the top of the atmosphere onto the first PC (W m^{-2} per standard deviation; labeled rtoa). (b) Regression of the AMOC onto the first PC (Sv per standard deviation; labeled amocss). (c) Regression of the total cloud fraction onto the first PC (% per standard deviation; labeled clt). (d) Regression of the heat content in the upper ocean onto the first PC (K per standard deviation; labeled ohc300). (e) Regression of the shortwave component of the cloud radiative effect onto the first PC (W m^{-2} per standard deviation; labeled cresw). (f) Regression of the longwave component of the cloud radiative effect onto the first PC (W m^{-2} per standard deviation; labeled crelw). The box in (c) marks the southeastern tropical Atlantic region, where the local relationship between several variables is calculated in Fig. 4. Gray contours mark regions where the regression is statistically significant.

decks of low-level marine stratocumulus (Karlsson et al. 2008) and coincides with decreased cloudiness in those areas (Fig. 3c). In the southeastern tropical Atlantic, most models underestimate cloud cover (Fig. 4c). As in previous works (Lauer and Hamilton 2013), this underestimation can be traced back to the atmospheric component (not shown). The models that strongly underestimate cloud cover in this region tend to show higher values of PC1

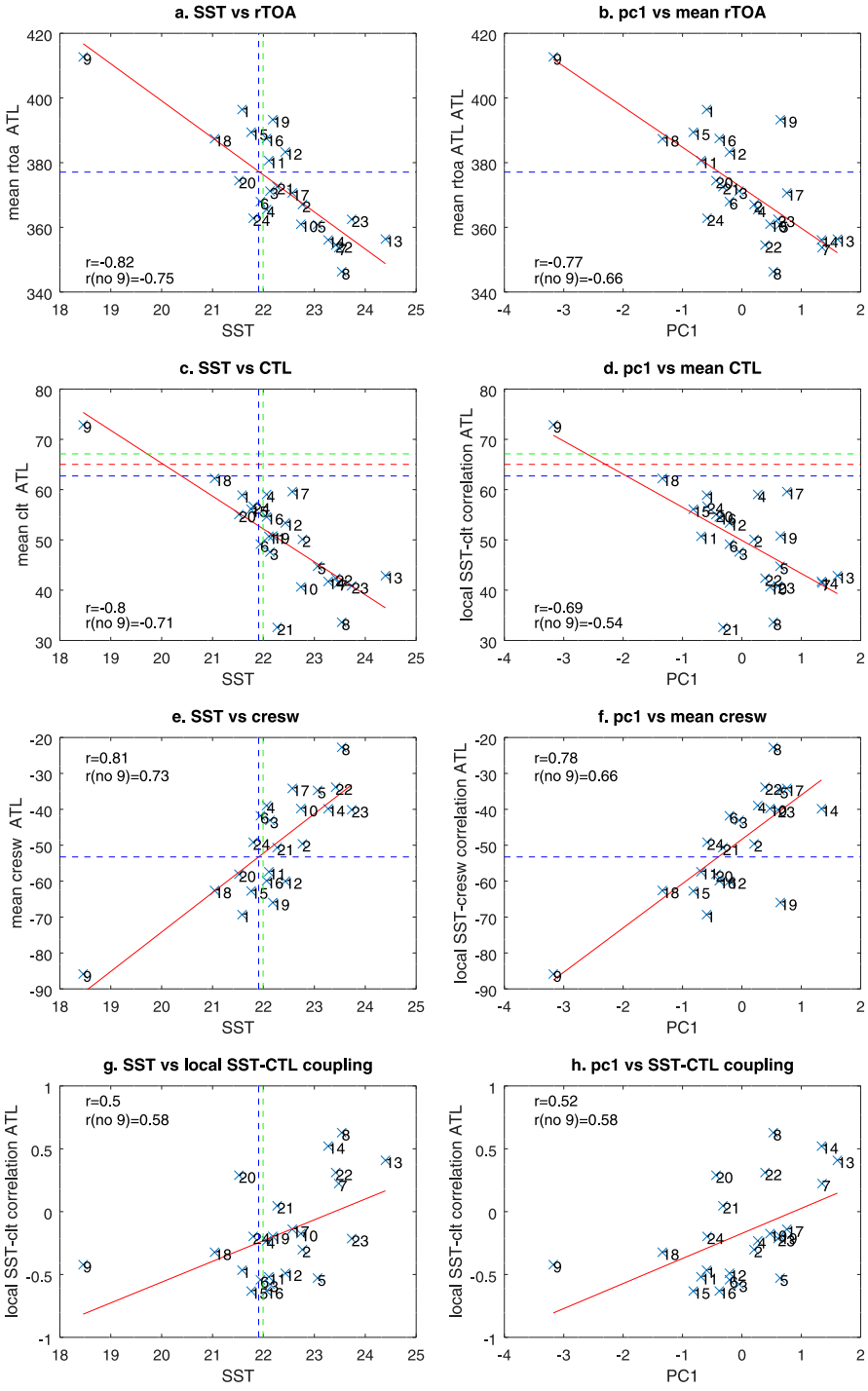

FIG. 4. Scatterplot of southeastern tropical Atlantic (sTA; 15°W–10°E, 25°–10°S; see box in Fig. 3c) (left) SSTs (K) and (right) PC1 (nondimensional) against (a),(b) the outgoing total radiation (longwave plus shortwave) at the top of the atmosphere ($W\,m^{-2}$; labeled rtoa) in sTA, (c),(d) the total cloud fraction (%) in sTA, (e),(f) the shortwave component of the cloud radiative effect ($W\,m^{-2}$; labeled cresw) in STA, and (g),(h) the local time correlation between SSTs and total cloud fraction in sTA. The red line shows the regression fit. Vertical blue (green) lines in the left panels show the observed estimate using HadISSTv1 (ERSSTv4) dataset. Horizontal dashed lines in (a), (b), (e), and (f) show the corresponding observed estimates using CERES climatological means (from July 2005 to June 2015). In (c) and (d) the observed climatological estimates of the cloud fractional cover obtained with ISCCP (1984–2007), AIRS-LMD (2003–09), and TOVS Path-B (1987–94) are shown as blue, red, and green horizontal dashed lines, respectively. Correlation values are shown in the left part of the panels are calculated with all models (r) and without model number 9.

and stronger SST warm biases (Figs. 4c,d). However, models for which the underestimation is moderate tend to display small local SST biases (Fig. 4c). This could be explained by the fact that models tend to show too strong albedo in the region (Engström et al. 2014), which would erroneously compensate the radiative effect of too weak cloud cover. Cloudiness also decreases in both the northern and southern extratropics. The pattern of shortwave cloud radiative effect associated with the first mode shows positive values over the eastern part of the basins and the extratropics, where cloudiness is decreased (Fig. 3e). In the southeastern tropical Atlantic, the climatological shortwave cloud radiative effect is negative (there is less outgoing shortwave radiation at the top of the atmosphere in clear-sky conditions than in all-sky conditions) (Fig. 4e) and its value tends to be underestimated, especially by those models that show a high value of PC1 and strong warm SST bias in the region (Figs. 4e,f). In turn, the anomalies in longwave cloud radiative effect show negative values in the extratropics and over the Maritime Continent (Fig. 3f). These results suggest that in the tropics the decrease of cloudiness in the eastern parts of the subtropical basins shown in Fig. 3c comes from reduced low-level clouds, which would decrease albedo strongly while not changing much the outgoing longwave radiation leading to a local radiative warming. Further analysis of cloud cover at low heights tends to confirm this (not shown). Conversely, the cloudiness decrease in the extratropics would be also related to high-level clouds, which would increase the outgoing longwave radiation (Fig. 3f). In the extratropics, the radiative effect of the decrease in low- and high-level cloudiness would cancel out except in the Southern Ocean around 60°S, where there is more net radiation loss to space and the effect of high clouds seem to dominate.

In Figs. 4g and 4h we show that models with a tendency to obtain colder SST climatologies in the southeastern tropical Atlantic (and more climatological low-level cloudiness) also tend to show a local negative correlation between cloudiness and SSTs. Such negative correlation suggests that a positive feedback involving SST and cloud cover, which characterizes marine stratocumulus, is at work in the region. That is, an increase in SSTs tends to be associated with a reduction in cloudiness leading to enhanced shortwave radiation into the ocean and a further increase in SSTs, consistently with observations (Lin et al. 2014). As there is a strong relationship between the southeastern tropical Atlantic SSTs and the strength of the PC (correlation −0.93), the models with high negative values of the PC are those in which the southeastern tropical Atlantic is a region mediated by stratocumulus effects. Conversely, strong positive values of the PC, which are consistent with climatological warmer SSTs in the southeastern tropical Atlantic (and less climatological low-level cloudiness), correspond to models that show a positive correlation between SSTs and total cloud cover. Such positive local correlation is characteristic of a region mediated by deep convection: An increase in SSTs leads to higher local wind convergence at the surface, ascending motion, and increased deep convection and cloudiness. Thus, the stronger the positive values of the PC, the stronger the model's failure in the simulation of the marine stratocumulus regime characteristic of the region, representing a southeastern tropical Atlantic behaving more as if it was a convective region. Roughly, two-thirds of the models display a negative correlation between cloudiness and SSTs in the tropical Atlantic (i.e., represent a stratocumulus mediated region). Roughly half of the models show a negative correlation in the south tropical Pacific (not shown), which broadly agrees with the results of Lin et al. (2014), who found that 3 out of 8 models showed a low cloud–SST feedback consistent with observations. Whether the high SSTs are the responsible for the misrepresentation of the observed cloud regime, or whether they are due to the failure in the simulation of the SST–cloud feedback, remains an open question.

b. *Second mode of intermodel spread in tropical Atlantic SSTs*

The second mode of intermodel spread in the tropical Atlantic projects onto an interhemispheric dipole of SSTs in the Atlantic basin (Fig. 5a). For models with positive values of the second PC (Fig. 5b) there are negative values in the north and positive ones, though not statistically significant, in the south (Fig. 5a). The strongest values of the PC associated with this second mode correspond to the CSIRO Mk3.6.0 (negative value) and NorESM1-M (positive value) models. The SST bias of both models shows an eastward gradient in the tropical South Atlantic consistent with EOF2 (Gordon et al. 2010; Koseki et al. 2018). However, unlike all other models, the CSIRO Mk3.6.0 model shows an SST bias with a northward gradient in the equatorial Atlantic, which is opposite to the one shown in EOF2 (Gordon et al. 2010). Noteworthy are the negative and statistically significant anomalies in the subpolar gyre region, suggesting there is a strong intermodel spread in the simulation of temperatures in that region, in accordance with Menary et al. (2015). This anomalous SST pattern is reminiscent of the one related to the Atlantic multidecadal variability, except for a stronger signature in the tropical North Atlantic (Kerr 2000; Knight et al. 2006; Zhang 2007; Ting et al. 2009, 2011; Ruprich-Robert et al. 2017). The fraction of variance explained by this second mode is 12.6%

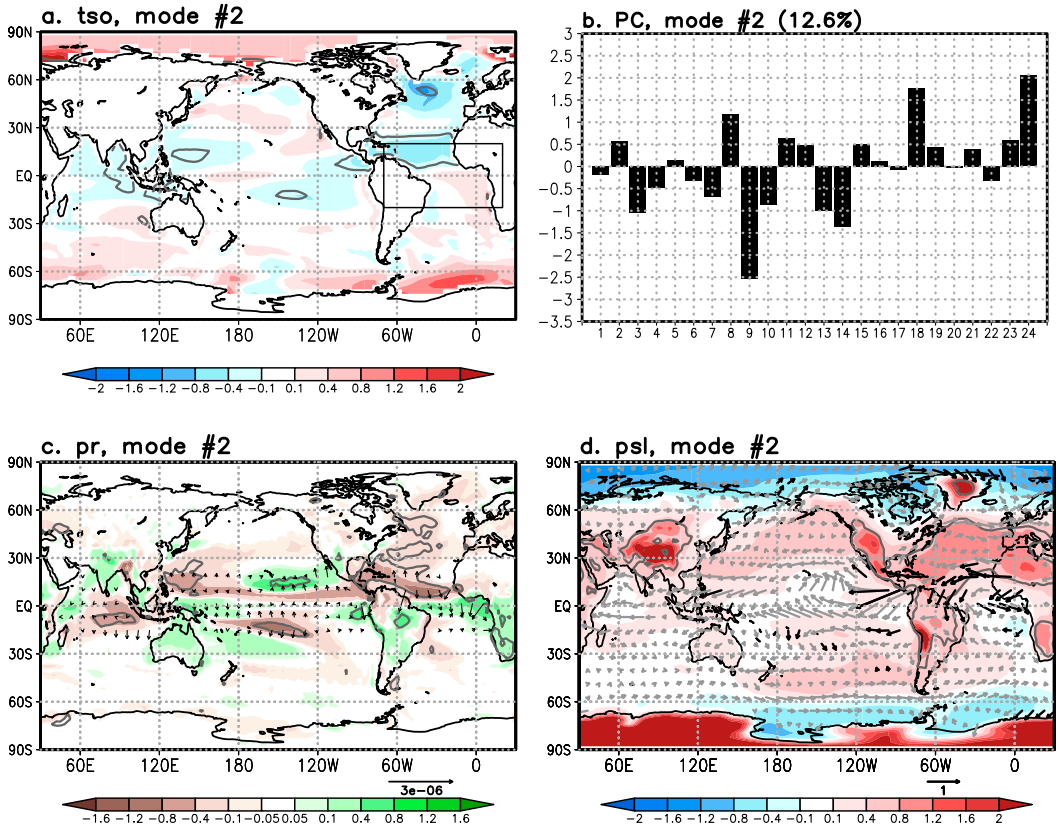

FIG. 5. As in Fig. 2, but for the second mode of intermodel variability in the tropical Atlantic.

and it is separated from the third one according to North's rule of thumb (North et al. 1982).

Unlike the first mode, the second mode is more restricted to the Atlantic basin. When the analysis is repeated taking into account the whole tropics (20°S–20°N) or the global SSTs between 60°S and 60°N the correlation between the original second PC (Fig. 5b) and the one obtained from these calculations is not statistically significant. Conversely, when the analysis is repeated for the Atlantic extending the latitudinal boundaries to 30°S–30°N or 40°S–40°N the correlations with the original second PC are 0.96 and 0.69, respectively (although in this case this mode appears as the third one), respectively. In these cases, the SST anomalies show more marked loads in the North Atlantic (not shown).

Along with the anomalous southward SST gradient in the tropical Atlantic, there is an anomalous northward sea level pressure gradient, with positive anomalies in the northern tropical Atlantic extending to southern Europe and northern Africa, suggestive of a positive NAO phase in the extratropics (Fig. 5d). In the tropical Atlantic, there are northeasterly (northwesterly) surface wind anomalies north (south) of the equator. Consistent with the southward SST gradient in the equator, rainfall is reduced to the north of the equator and enhanced to the south, suggesting a more southward location of the Atlantic ITCZ (Fig. 5c).

Although somewhat consistent with the SST pattern, the anomalies in the net outgoing radiation at the top of the atmosphere for the second mode cannot explain those in SSTs (Fig. 6a). In contrast, there is a clear signal in the projection of the AMOC onto the PC associated with the second mode (Fig. 6b). These statistically significant negative AMOC anomalies in the central Atlantic become even more prominent when the analysis is repeated with the northern boundary of the region moved poleward (not shown). There is also a negative signal in the subpolar gyre upper-ocean heat content (Fig. 6d). A weakened AMOC reduces warm surface water transport to the North Atlantic, leading to cold anomalies there (Knight et al. 2005; Dima and Lohmann 2007; Lu and Dong 2008; Persechino et al. 2012; Zhang and Wang 2013). In addition, a heat budget analysis suggests that most of the North Atlantic cooling associated with this mode is related to the ocean residual, especially in the subpolar gyre region (see section 1.2 in the online supplemental material). The cold SST signal in the tropical Atlantic could be related to the enhanced subtropical North Atlantic

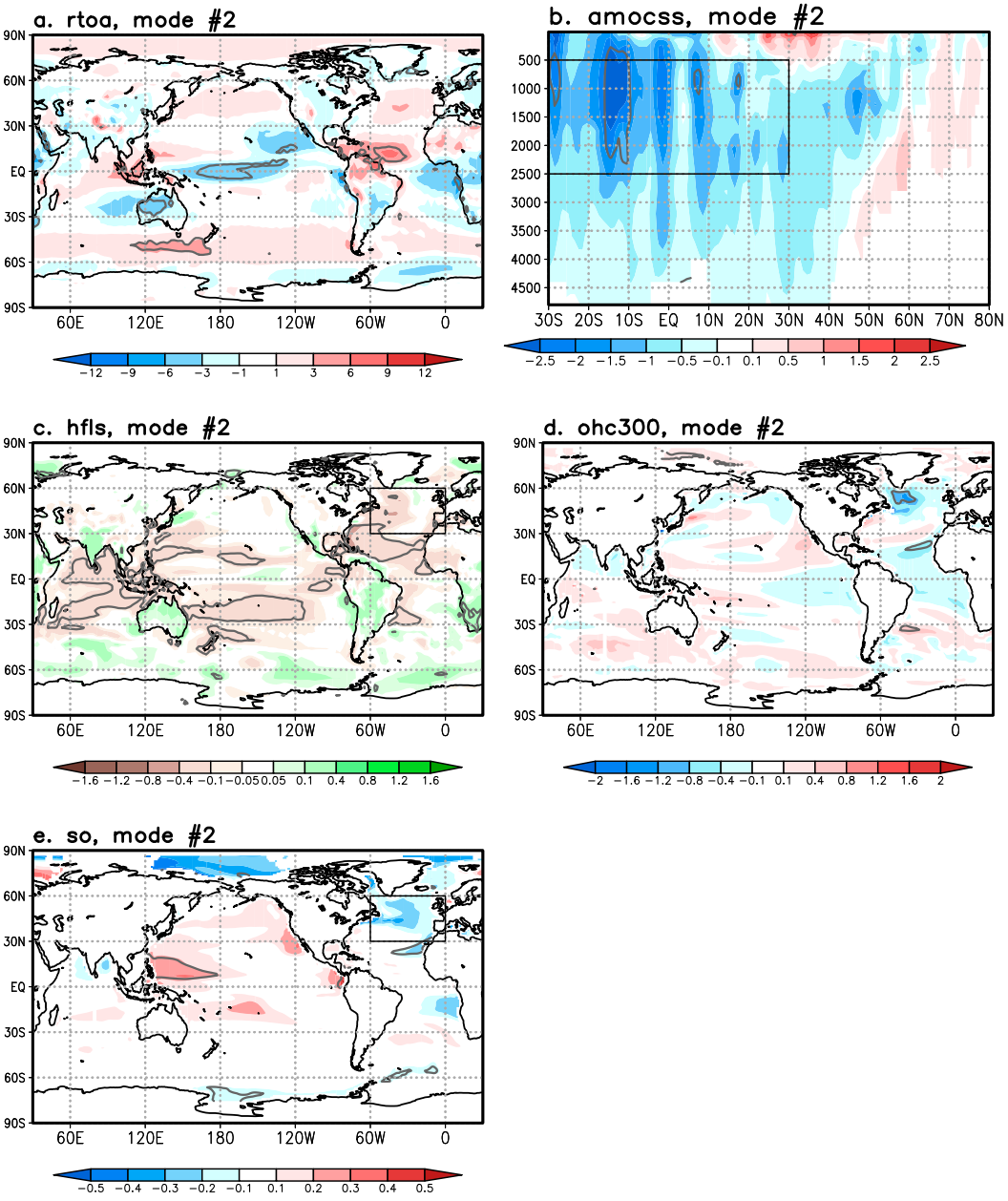

FIG. 6. Possible causes for the second mode of intermodel variability in the tropical Atlantic: (a) regression of outgoing total radiation (longwave plus shortwave) at the top of the atmosphere onto the second PC (W m^{-2} per standard deviation; labeled rtoa); (b) regression of the AMOC onto the second PC (Sv per standard deviation; labeled amocss); (c) regression of the evaporation onto the second PC (mm day^{-1} per standard deviation; labeled hfls); (d) regression of the heat content in the upper ocean onto the second PC (K per standard deviation; labeled ohc300); and (e) regression of the salinity in the mixed layer (15-m depth) onto the second PC (psu per standard deviation; labeled so). The box in (b) marks the region used to calculate the AMOC index in Fig. 7a. The boxes in (c) and (e) mark the North Atlantic region used to calculate evaporation and upper ocean salinity in Fig. 7. Gray contours mark regions where the regression is statistically significant.

overturning cell (Fig. 6b), which could bring intensified upwelling and poleward Ekman transport at this latitude in response to the intensified trade winds (Fig. 5b). This is, in fact, a footprint of the AMOC on the tropical Atlantic SSTs as discussed by Zhang (2007). Therefore, our results strongly suggest that the SST anomalies in Fig. 5a are related to a weakening of the AMOC and are consistent with the described impacts of AMOC changes on SST.

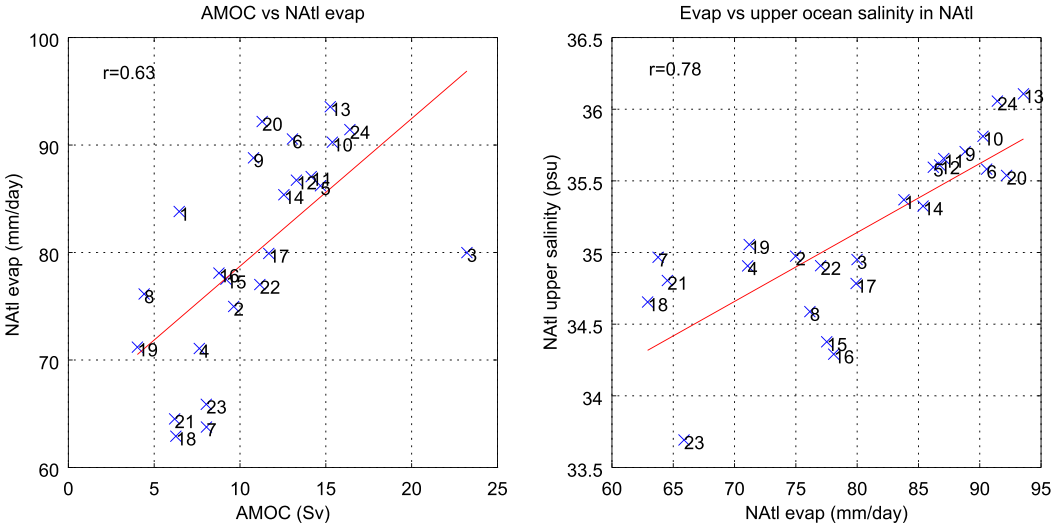

FIG. 7. Feedback between AMOC and North Atlantic (Natl; 60°W–0°E, 30°–60°N; see box in Figs. 6c,e) evaporation and salinity in the mixed layer (15-m depth). (a) Scatterplot of AMOC (Sv; taken as the average value in the area 30°S–30°N, 500–2500-m depth; see Fig. 6b) vs evaporation (mm day^{-1}) in the North Atlantic. (b) Scatterplot of North Atlantic evaporation (mm day^{-1}) vs salinity (psu) in the mixed layer (15-m depth). The red line shows the regression fit. Correlation values are shown in the top left part of each panel.

Menary and Scaife (2014) suggested that a weaker AMOC occurs through a lighter (reduced density) North Atlantic surface water driven by anomalous high surface freshwater fluxes due to reduced evaporation. Consistently with this, the second mode of intermodel spread shows decreased evaporation in the North Atlantic together with reduced salinity in the upper ocean over the subpolar part (Figs. 6c,f). Such negative anomalies in salinity of the North Atlantic Ocean extend in depth up to 1500 m (not shown). Moreover, Cheng et al. (2013) suggested a positive feedback between AMOC and North Atlantic surface salinity. In this feedback, a decrease in the AMOC would be associated with colder SSTs and reduced evaporation in the North Atlantic, leading to a local freshening and decrease in surface density, which would further weaken the AMOC. This mechanism seems to operate in the simulations, as shown in Fig. 7. That is, those models with weaker AMOC tend to show reduced evaporation in the North Atlantic and lower surface salinity. However, anomalies of surface salinity and evaporation associated with the second mode are weak (Figs. 6c,f). In addition, there is reduced rainfall associated with this mode in the subpolar gyre region (Fig. 5c), although the overall effect of precipitation and evaporation is a freshening of the area (not shown).

c. *Third mode of intermodel spread in tropical Atlantic SSTs*

The third mode of intermodel spread in the tropical Atlantic projects onto a worldwide interhemispheric dipole-like pattern in SST (Fig. 8a): Positive values of the PC are associated with negative anomalies in the Northern Hemisphere, especially in the subpolar and polar regions where values are statistically significant, and positive anomalies in the Southern Hemisphere, especially over the subtropical regions, with statistically significant anomalies in the Atlantic and eastern Pacific basins. Over the equator, the SST show negative anomalies in the eastern part of the Pacific, Atlantic, and Indian basins. This third mode explains only 8.4% of intermodel variance of tropical Atlantic SST. It is separated from the fourth according to North's rule of thumb (North et al. 1982).

As with the first mode, the third mode is also found when the EOF analysis is repeated in different regions. The correlations of the original PC (Fig. 8b) and the third PC obtained from the EOF calculation applied to the whole tropics (20°S–20°N) or the global SSTs between 60°S and 60°N are 0.58, and 0.63, respectively. In addition, the third mode seems to be more dominant in the tropical Pacific east of the date line (180°–80°W, 20°S–20°N), where it appears as the second one (the correlation between the second PC in the tropical Pacific and the third one in the tropical Atlantic is 0.64) explaining approximately 15% of intermodel variance there.

The rainfall anomalies associated with the third mode show strong and statistically significant values in the tropics and subtropics (Fig. 8c). They tend to show consistency with the SST pattern whereby positive

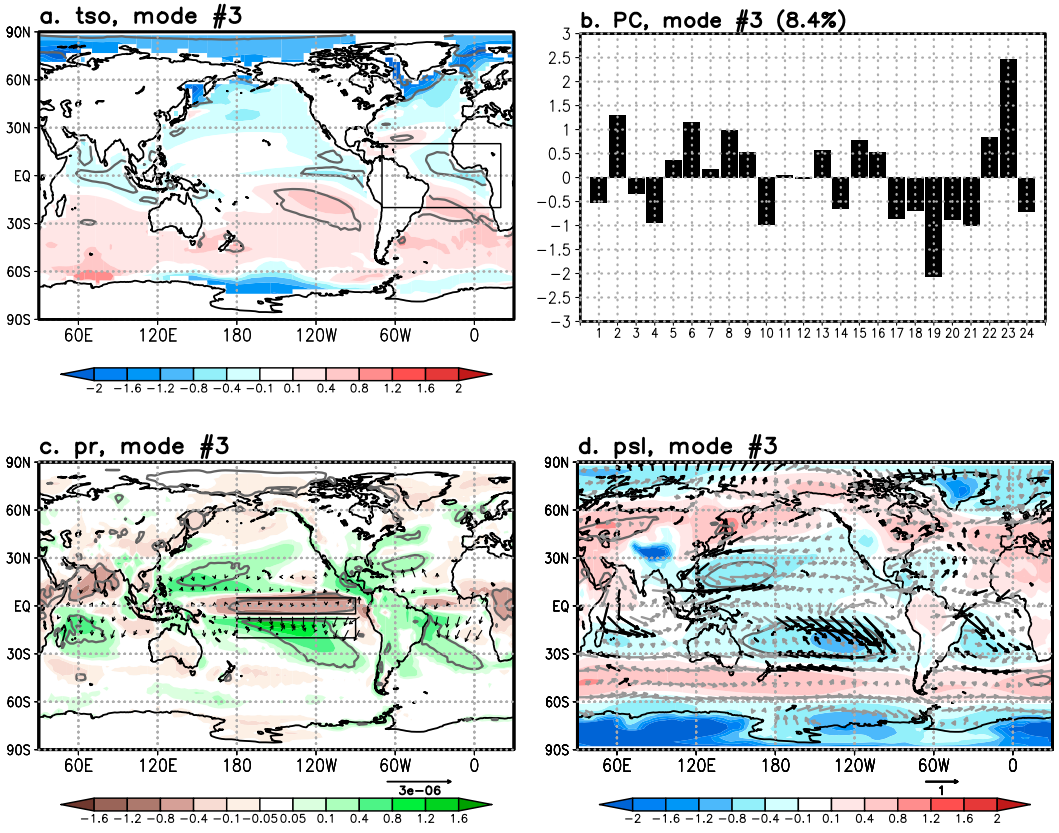

FIG. 8. As in Fig. 2, but for the third mode of intermodel variability in the tropical Atlantic.

(negative) rainfall anomalies are located over warm (cold) SST ones (Fig. 8a). Rainfall is reduced in the equatorial band, especially over the Pacific. There are also negative anomalies over the Arabian Sea and India and over central Africa. Off the equator, in the tropics and subtropics, there are positive rainfall anomalies over the western oceans, except for the South Pacific, where positive anomalies extend from the central tropics eastward up to 90°W, strengthening the South Pacific convergence zone. The positive tropical and subtropical anomalies are more intense in the Southern than in the Northern Hemisphere, providing an overall southward shift of the ITCZ, which is more intense in the Pacific basin and is consistent with the southward gradient of SSTs. Consistently with the rainfall anomalies, there are surface cyclones located over the western subtropical oceans (Fig. 8d).

This third mode seems to have, at least in part, an atmospheric origin. There is no statistically significant signal in salinity or in temperature in the deep ocean below 1000-m depth in any basin (not shown) and the projection of the AMOC onto the PC shows no clear signal (Fig. 9b). To find some explanation on the tropical SST pattern associated with this mode we examine the net outgoing radiation at the top of the atmosphere (Fig. 9a). There is less loss of net radiation to space (negative anomalies) off the equator in the tropics approximately over the regions where SST and rainfall anomalies are positive. This is further confirmed by a heat budget analysis of the ocean mix layer that suggests that the increase of shortwave radiation into the ocean could be linked to the local warm SST anomalies (see section 1.3 in the online supplemental material). However, the negative SST anomalies in the eastern equatorial Pacific and Atlantic Oceans seem related to the ocean residual term in the heat budget analysis (see section 1.3 in the online supplemental material).

The southern shift of the ITCZ, especially over the tropical Pacific, and the plausibility of explaining the third mode of intermodel spread based on the radiation budget at the top of the atmosphere, suggests a relationship with the strength of the double ITCZ (DI) bias shown by models. In Fig. 10a we use as an estimate of the tropical Pacific DI the difference between the south tropical (180°–90°W, 20°–8°S) and equatorial (180°–90°W, 5°S–5°N) rainfall to show there is a link with the third PC. Xiang et al. (2017) further showed that the DI problem was related to the atmospheric north–south

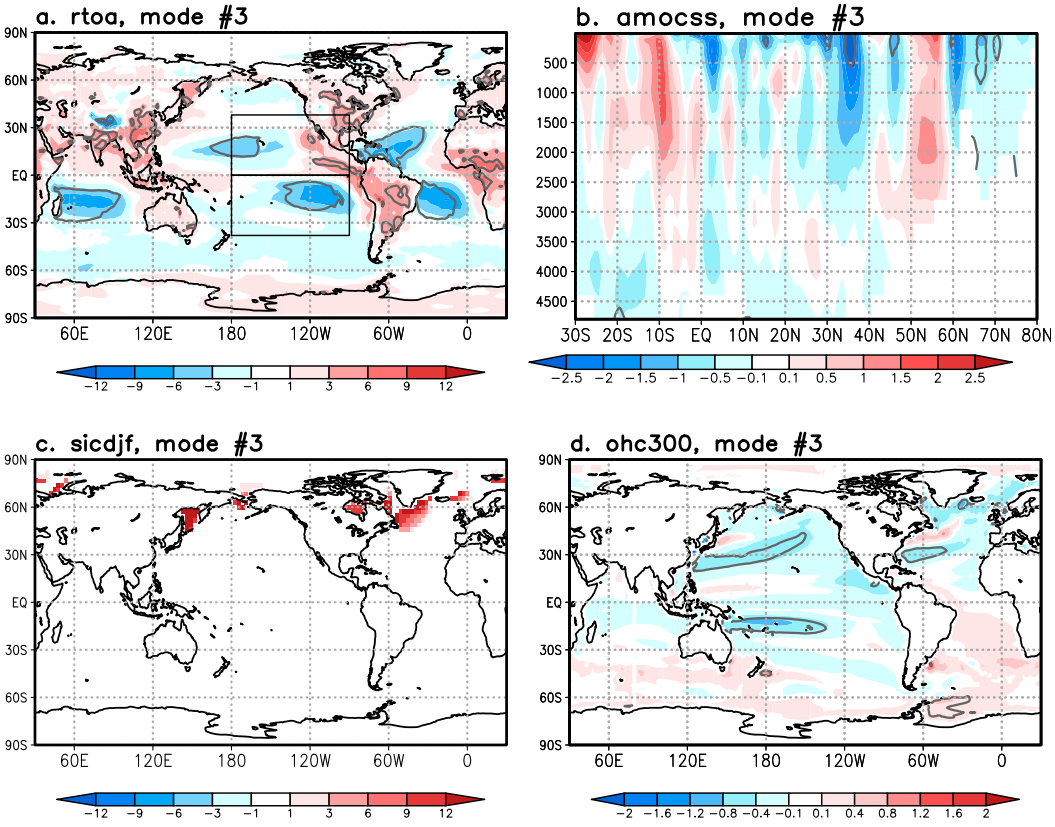

FIG. 9. Possible causes for the third mode of intermodel variability in the tropical Atlantic. (a) Regression of outgoing total radiation (longwave plus shortwave) at the top of the atmosphere onto the third PC (W m^{-2} per standard deviation; labeled as rtoa). (b) Regression of the AMOC onto the third PC (Sv per standard deviation; labeled as amocss). (c) Regression of the sea ice cover in the December to February season onto the third PC (% per standard deviation; labeled as sicdjf). (d) Regression of the heat content in the upper ocean onto the third PC (K per standard deviation; labeled as ohc300). Gray contours mark regions where the regression is statistically significant. For the sea ice cover only statistically significant anomalies are drawn. Boxes in (a) show the areas used to calculate the asymmetry of the top of the atmosphere net radiation flux in the tropical Pacific shown in Fig. 10b.

asymmetry in tropical radiation at the top of the atmosphere in the atmospheric component of the models. Figure 10b confirms that there is a connection between the asymmetry in the net radiation at the top of the atmosphere and the PC.

The strong negative surface temperature anomalies in the polar and subpolar regions associated with the third mode are related to the increase in sea ice cover, especially in boreal winter (Fig. 9c) and spring (not shown). Replacing open ocean by sea ice leads to a strong cooling in surface temperatures (Fig. 8a). In addition, positive anomalies in sea ice cover are also related with a local increase in shortwave radiation loss to space in clear-sky conditions (not shown), which is consistent with the high albedo of sea ice surface and that leads to a further local cooling.

In the upper ocean, heat content is reduced over the western North Pacific and Atlantic and over the southern tropical Pacific (Fig. 9d). These negative anomalies tend to coincide with lower SSTs. There are only two exceptions for this: the western North Atlantic off Newfoundland, and the southern tropical Pacific between 180° and 120°W. In the latter case, the warm anomalies in the ocean remain above 50-m depth, while there are cold anomalies farther down (Fig. 11b). An explanation for this decoupling of SST and upper ocean temperature can be found in the salinity anomalies (Fig. 11a): The increased rainfall in the area freshens the upper ocean leading to an increase in the ocean column stability. This behavior is also observed in the case of the western North Atlantic (not shown).

d. Relationships between the first three modes and tropical Atlantic SST bias

In the previous sections we have analyzed the spread in the simulation of tropical Atlantic SST biases and we

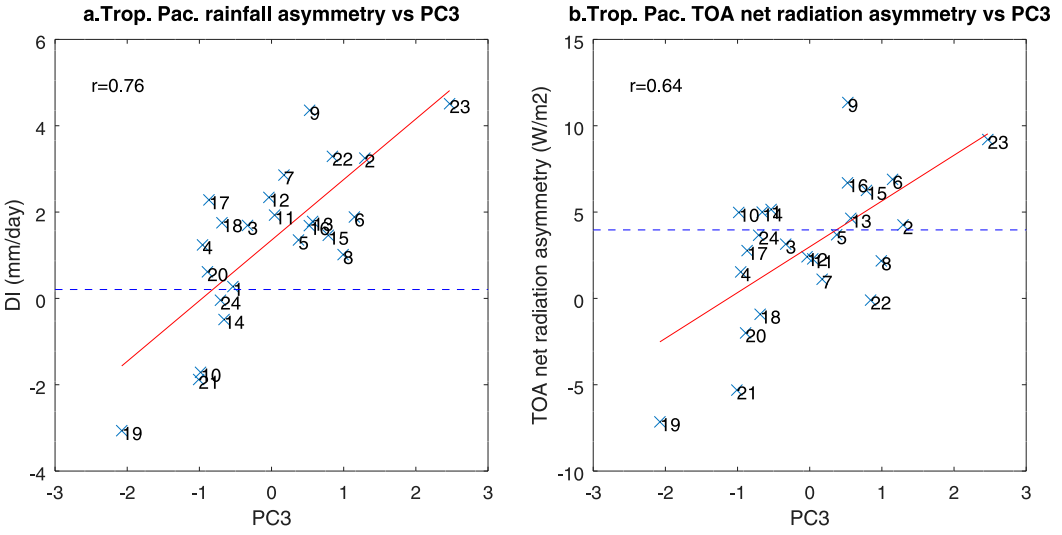

FIG. 10. Link between the third PC and the Pacific double-ITCZ (DI) problem. (a) Scatterplot of the third PC (nondimensional) and the DI (mm day^{-1}) defined as the difference in precipitation between the south tropical Pacific (180°–90°W, 20°–8°S) and equatorial Pacific (180°–90°W, 5°S–5°N) (see boxes in Fig. 8c). (b) Scatterplot of the third PC (nondimensional) and the asymmetry of top of the atmosphere net radiation flux (W m^{-2}) in the tropical Pacific, defined as the difference between the northern (180°–90°W, 0°–38°N) and southern (180°–90°W, 38°S–0°) tropical Pacific (see boxes in Fig. 9a). The red line shows the regression fit. The horizontal dashed line in (a) shows the corresponding observed estimates using GPCP v2.3 climatological means in the 1979–2017 period. The horizontal dashed line in (b) shows the corresponding observed estimates using CERES climatological means (from July 2005 to June 2015). Correlation values are shown in the top left part of the plot.

have related it to the differences in the simulation of low cloud cover, AMOC strength, and the double ITCZ in the Pacific. However, the causes for spread in model biases could be different from the causes of the mean state biases, so in this section we evaluate to what extent the main modes of intermodel spread resemble the mean SST bias shown in Fig. 1a. The spatial correlation between the mean bias and the SST projected onto each of the three first PCs (Figs. 2a, 5a, and 8a) is shown in Table 3. The greatest resemblance to the mean bias pattern corresponds to the second mode, followed by the third (with a change of sign) and first modes.

Taking all three modes of intermodel spread together into account, we evaluate the contribution of each mode to the structure of the mean bias by performing a spatial multilinear regression fit of the mean bias using the projected SSTs on each of the three PCs (Figs. 2a, 5a, and 8a). We restrict the fit to the grid points belonging to

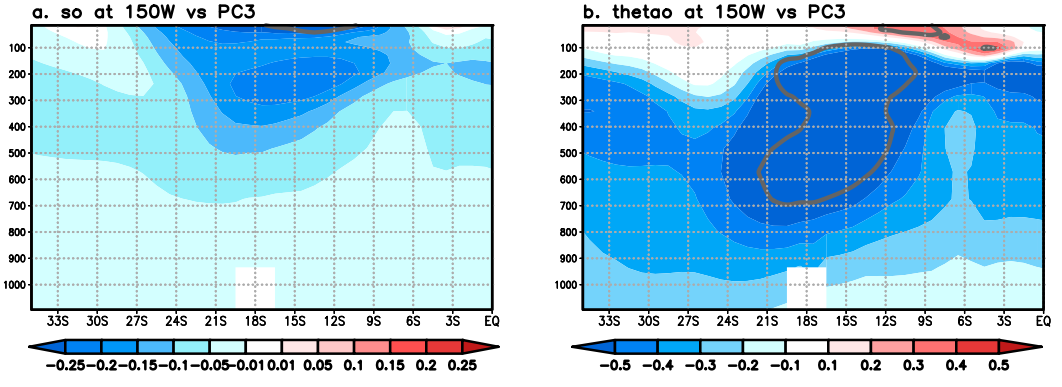

FIG. 11. South tropical Pacific upper-ocean salinity and temperature related to the third PC. (a) Intermodel regression of upper-ocean salinity (psu per standard deviation) at 150°W onto the third PC as a function of depth and latitude. (b) Intermodel regression of upper ocean seawater potential temperature (K per standard deviation) at 150°W onto the third PC as a function of depth and latitude. Gray contours mark regions where the regression is statistically significant.

TABLE 3. Spatial correlation between the mean bias and the SST projection onto each of the first three PCs in the tropical Atlantic (first column). Percentage of spatial variability of the bias in the tropical Atlantic explained separately by each mode in the multilinear fit (second column). Coefficients of the multilinear regression fit with no intercept between the SST bias in the tropical Atlantic and the projection of the SST onto the PCs of the three first modes of intermodel spread in SST (third column; $K\,K^{-1}$).

	Spatial correlation with mean bias	Percent of variance explained by the fit	Coefficients of the fit
PC1	0.38	1.5	0.05 ± 0.13
PC2	0.76	54	2.63 ± 0.29
PC3	−0.43	16	−1.67 ± 0.36

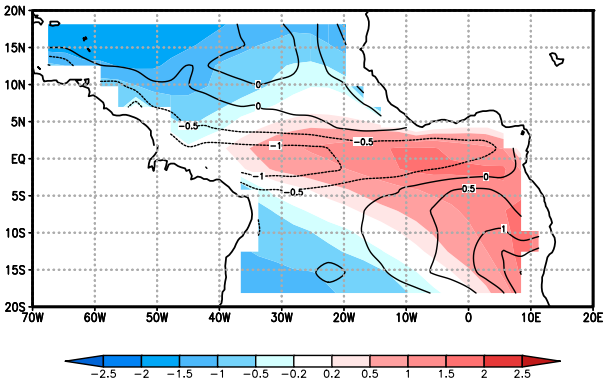

FIG. 12. Tropical Atlantic SST bias. Reconstructed bias using the coefficients of the spatial multilinear fit to the mean bias and the projections of the three first modes of intermodel spread in Figs. 2a, 5a, and 8a (see text for details) in shading (K). Difference between the mean bias in Fig. 1a and the reconstructed one in contours (K).

the tropical Atlantic region. Such a model explains above 70% of the spatial variance of the mean bias of the region. The coefficients of the fit and an estimate of the percentage of variance explained by each mode in the fit are shown in Table 3. The second mode dominates the fit, followed by the third one. The coefficients for the first mode are very small and, thus, the mode explains very little spatial variance. To evaluate if this mode was an unnecessary factor in the multilinear regression, we applied a stepwise regression (von Storch and Zwiers 2003). The analysis suggested that the contribution of this mode to the total variance, though small, was statistically significant at the 1% level, so it was retained in the analysis. Using the coefficients of the fit and the SST projections we reconstruct the fit to the bias (Fig. 12, shaded). According to Fig. 12, a simple linear model captures the overall mean bias pattern, showing a cold bias in the western Atlantic and a warm one in the eastern. However, as highlighted by the difference between the mean bias and the fitted one (Fig. 12, contours), the fit does not manage to explain the strong warm bias in the southeastern tropical Atlantic. It also fails to explain the western equatorial cold bias, showing a reduced west to east SST gradient in the equator.

4. Discussion

An analysis of the first three modes of SST intermodel variability in the tropical Atlantic suggests an important role for nonlocal processes in the origin of this variability. The first mode is related to the models' success in simulating low-level cloudiness in the marine subtropics. The second mode is related to the strength of the simulated AMOC, while the third mode seems primarily related to the strength of the double ITCZ bias in the tropical Pacific.

As indicated in the introduction, there are many studies that point to a local origin of the biases in the tropical Atlantic SSTs, especially the ones related to the too warm southeastern tropical Atlantic and the too weak cold tongue (e.g., Breugem et al. 2008; Richter et al. 2012; Zermeño-Diaz and Zhang 2013; Toniazzo and Woolnough 2014; Xu et al. 2014; Voldoire et al. 2014; Richter et al. 2015; Hourdin et al. 2015). The approach taken in this work by calculating the EOFs in the whole tropical Atlantic might prevent very local mechanisms to appear as prominent because they would only explain intermodel spread in small regions. A plausible way to reconcile the local and nonlocal views can be found when comparing the mean bias and the reconstructed one using the spatial multilinear fit (Fig. 12). The main differences between both lie in the equatorial Atlantic and in the southeastern tropical Atlantic, where other local effects could dominate.

Our estimate of the multilinear fit of the mean bias by the first three EOFs suggests that the main factor controlling the tropical Atlantic bias pattern is the second mode. This is, those models that simulate a too weak AMOC will tend to show a more pronounced bias in the tropical Atlantic, in accordance with Wang et al. (2014). This finding is also supported by results from water-hosing experiments, in which the SST anomaly generated by a shutdown of the AMOC, which closely resemble the SST pattern of the second mode in the Atlantic basin, have also important similarities with the mean bias pattern of CMIP5 models in terms of SST gradients in the tropical Atlantic (Timmermann et al. 2007; Wu et al. 2008; Liu et al. 2015). In addition, those models that tend to have a pronounced double ITCZ problem in the tropical Pacific (positive values of the third PC) will tend to show less SST bias in the tropical Atlantic. The first mode that accounts for most of the intermodel variance not only in the tropical Atlantic but also worldwide does not seem to be highly relevant to

explain the spatial pattern of the mean bias in the tropical Atlantic. As this mode is related to the amount of low-level cloudiness simulated by the models our result seem to suggest that, contrary to previous studies (Huang et al. 2007; Hu et al. 2008), the underrepresentation of the low-level stratocumulus deck over the south tropical Atlantic is not key for the overall spatial pattern of the bias there. A possible explanation is that the underrepresentation of the low-level cloud deck in a model does not take place only in the tropical Atlantic but rather is also a problem in other marine stratocumulus regions. The overall effect is a warming of the whole tropics with not very pronounced SST gradients (Fig. 2a).

5. Summary and conclusions

Our aim in the present paper is to increase the understanding of the reasons for intermodel spread in the representation of climatological SSTs in the tropical Atlantic and to relate it to the mean biases in the region. Our approach started with an analysis of the main modes of intermodel spread in the region. We demonstrated that most of the intermodel variance can be obtained with only the first three modes, which together account for over 85% of the variance.

The first mode of intermodel spread in SSTs explains 65% of this spread and is associated with differences in the simulated amount of low-level clouds over the eastern parts of the subtropical basins. Those models that simulate less marine low-level clouds have smaller albedo and shortwave radiation out of the atmosphere, which result in a warming of the tropical SSTs especially over the eastern part of the basins. Such a warming enhances the upper-ocean heat content. In the tropical Atlantic, the warming is more effective in the south than in the north, leading to a weaker St. Helena anticyclone, weakened surface northward cross-equatorial flow, and southward shift of the ITCZ. In addition, those models that show colder SSTs in the south tropical Atlantic (stronger negative values of the PC) are those that tend to simulate a positive feedback between SSTs and total cloud cover, characteristic of regions where stratocumulus decks are dominant. Conversely, those models that show warmer SSTs in the south tropical Atlantic (strong positive values of the PC) are those that tend to simulate the region as characterized by deep convection, where an increase of SSTs leads to higher convection and more high-level cloudiness. Our results therefore suggest that the main cause for the intermodel spread in tropical Atlantic SSTs is related to the intermodel spread in cloud cover, which can be traced back to the representation of cloud properties in the atmospheric component (Lauer and Hamilton 2013).

The second mode of intermodel spread of SST in the tropical Atlantic is mainly related to the strength of the AMOC. Models with a weaker AMOC tend to show negative Atlantic multidecadal variability (AMV)-type anomalies (colder and warmer SSTs in the North and South Atlantic, respectively), which promote higher surface pressure in the north and a shift of the ITCZ location toward the equator. The reasons for the simulation of a weak AMOC can be related to an evaporation–surface salinity–AMOC strength positive feedback in the North Atlantic, by which a weakened AMOC reduces North Atlantic SSTs decreasing evaporation. This, in turn, leads to reduced upper ocean salinity and further weakening the AMOC. Although the second mode is also related to reduced rainfall in the subpolar gyre region, the overall effect of precipitation and evaporation is a freshening of the area.

The third mode of intermodel spread is characterized by an interhemispheric SST gradient, with cold anomalies in the Northern Hemisphere and in the eastern equatorial oceans and warm anomalies to the south. We have argued that the main explanation for such a configuration of the SSTs is related to the outgoing net radiation at the top of the atmosphere, which shows reduced loss of net radiation in the subtropics, especially in the Southern Hemisphere, leading to a local warming. Conversely, ocean processes lead to an equatorial cooling. Such a SST configuration leads to a southern shift of the ITCZ. This mode seems related to the strength of the double-ITCZ bias in models, especially over the tropical Pacific.

Through a spatial multilinear fit to the mean bias in tropical Atlantic SST using the three analyzed modes, we find that the main contributor by large to exacerbating the bias pattern is the second mode. This suggests that those models that fail at simulating a strong AMOC will tend to show stronger biases in the tropical Atlantic. Our results also show that the first mode, although explaining the largest part of intermodel spread in climatological SSTs worldwide, does not project strongly on the tropical Atlantic bias. A possible explanation for this result is that the failure to simulate enough low cloud cover in the south tropical Atlantic in a model is not a problem particular to the Atlantic. In fact, models that underrepresent cloud cover there also fail in other maritime regions where stratocumulus prevail in observations. In general, these errors lead to a global warming, and do not project onto strong zonal SST gradients as the ones shown by the mean bias.

Acknowledgments. This work was supported by the European Union Seventh Framework Programme (FP7/2007-2013) under Grant Agreement 603521 and

the Spanish Project CGL2017-86415-R. We acknowledge the World Climate Research Programme's Working Group on Coupled Modelling, which is responsible for CMIP, and the climate modeling groups (listed in Table 1) for producing and making available their model output. For CMIP the U.S. Department of Energy's Program for Climate Model Diagnosis and Intercomparison provides coordinating support and led development of software infrastructure in partnership with the Global Organization for Earth System Science Portals. The work of CRM was funded by NOAA's Climate Program Office, Climate Variability and Predictability Program Award NA14OAR4310278. TL was supported with funds from the Juan de la Cierva-Incorporación Programme (IJCI-2015-26645).

REFERENCES

Adler, R. F., and Coauthors, 2003: The version-2 Global Precipitation Climatology Project (GPCP) monthly precipitation analysis (1979–present). *J. Hydrometeor.*, **4**, 1147–1167, https://doi.org/10.1175/1525-7541(2003)004<1147:TVGPCP>2.0.CO;2.

Bellucci, A., S. Gualdi, and A. Navarra, 2010: The double-ITCZ syndrome in coupled general circulation models: The role of large-scale vertical circulation regimes. *J. Climate*, **23**, 1127–1145, https://doi.org/10.1175/2009JCLI3002.1.

Breugem, W. P., P. Chang, C. J. Jang, J. Mignot, and W. Hazeleger, 2008: Barrier layers and tropical Atlantic SST biases in coupled GCMs. *Tellus*, **60A**, 885–897, https://doi.org/10.1111/j.1600-0870.2008.00343.x.

Cabos, W., and Coauthors, 2017: The South Atlantic Anticyclone as a key player for the representation of the tropical Atlantic climate in coupled climate models. *Climate Dyn.*, **48**, 4051–4069, https://doi.org/10.1007/s00382-016-3319-9.

Cheng, W., J. C. Chiang, and D. Zhang, 2013: Atlantic meridional overturning circulation (AMOC) in CMIP5 models: RCP and historical simulations. *J. Climate*, **26**, 7187–7197, https://doi.org/10.1175/JCLI-D-12-00496.1.

Danabasoglu, G., and Coauthors, 2014: North Atlantic simulations in coordinated ocean-ice reference experiments phase II (CORE-II). Part I: Mean states. *Ocean Modell.*, **73**, 76–107, https://doi.org/10.1016/j.ocemod.2013.10.005.

Davey, M., and Coauthors, 2002: STOIC: A study of coupled model climatology and variability in tropical ocean regions. *Climate Dyn.*, **18**, 403–420, https://doi.org/10.1007/s00382-001-0188-6.

Diakhaté, M., A. Lazar, G. de Coëtlogon, and A. T. Gaye, 2018: Do SST gradients drive the monthly climatological surface wind convergence over the tropical Atlantic? *Int. J. Climatol.*, **38**, e955–e965, https://doi.org/10.1002/joc.5422.

Dima, M., and G. Lohmann, 2007: A hemispheric mechanism for the Atlantic multidecadal oscillation. *J. Climate*, **20**, 2706–2719, https://doi.org/10.1175/JCLI4174.1.

Ding, H., R. J. Greatbatch, M. Latif, and W. Park, 2015: The impact of sea surface temperature bias on equatorial Atlantic interannual variability in partially coupled model experiments. *Geophys. Res. Lett.*, **42**, 5540–5546, https://doi.org/10.1002/2015GL064799.

Dippe, T., R. J. Greatbatch, and H. Ding, 2018: On the relationship between Atlantic Niño variability and ocean dynamics. *Climate Dyn.*, **51**, 597–612, https://doi.org/10.1007/s00382-017-3943-z.

Engström, A., F. A. M. Bender, and J. Karlsson, 2014: Improved representation of marine stratocumulus cloud shortwave radiative properties in the CMIP5 climate models. *J. Climate*, **27**, 6175–6188, https://doi.org/10.1175/JCLI-D-13-00755.1.

Flato, G., and Coauthors, 2013: Evaluation of climate models. *Climate Change 2013: The Physical Science Basis*, T. F. Stocker et al., Eds., Cambridge University Press, 741–866.

Gordon, H. B., S. O'Farrell, M. Collier, M. Dix, L. Rotstayn, E. Kowalczyk, T. Hirst, and I. Watterson, 2010: The CSIRO Mk3.5 climate model. CAWCR Tech. Rep. 021, 74 pp., https://www.cawcr.gov.au/technical-reports/CTR_021.pdf.

Goubanova, K., E. Sanchez-Gomez, C. Frauen, and A. Voldoire, 2019: Respective roles of remote and local wind stress forcings in the development of warm SST errors in the South-Eastern Tropical Atlantic in a coupled high-resolution model. *Climate Dyn.*, **52**, 1359–1382, https://doi.org/10.1007/s00382-018-4197-0.

Hourdin, F., A. Găinusă-Bogdan, P. Braconnot, J. L. Dufresne, A. K. Traore, and C. Rio, 2015: Air moisture control on ocean surface temperature, hidden key to the warm bias enigma. *Geophys. Res. Lett.*, **42**, 10 885–10 893, https://doi.org/10.1002/2015GL066764.

Hu, Z.-Z., B. Huang, and K. Pegion, 2008: Low cloud errors over the southeastern Atlantic in the NCEP CFS and their association with lower-tropospheric stability and air–sea interaction. *J. Geophys. Res.*, **113**, D12114, https://doi.org/10.1029/2007JD009514.

Huang, B., Z.-Z. Hu, and B. Jha, 2007: Evolution of model systematic errors in the tropical Atlantic basin from coupled climate hindcasts. *Climate Dyn.*, **28**, 661–682, https://doi.org/10.1007/s00382-006-0223-8.

Hwang, Y.-T., and D. M. W. Frierson, 2013: Link between the double-Intertropical Convergence Zone problem and cloud biases over the Southern Ocean. *Proc. Natl. Acad. Sci. USA*, **110**, 4935–4940, https://doi.org/10.1073/pnas.1213302110.

Jiang, J. H., and Coauthors, 2012: Evaluation of cloud and water vapor simulations in CMIP5 climate models using NASA "A-Train" satellite observations. *J. Geophys. Res.*, **117**, D14105, https://doi.org/10.1029/2011JD017237.

Kajtar, J. B., A. Santoso, S. McGregor, M. H. England, and Z. Baillie, 2018: Model under-representation of decadal Pacific trade wind trends and its link to tropical Atlantic bias. *Climate Dyn.*, **50**, 1471–1484, https://doi.org/10.1007/s00382-017-3699-5.

Kang, S. M., I. M. Held, D. M. W. Frierson, and M. Zhao, 2008: The response of the ITCZ to extratropical thermal forcing: Idealized slab-ocean experiments with a GCM. *J. Climate*, **21**, 3521–3532, https://doi.org/10.1175/2007JCLI2146.1.

Karlsson, J., G. Svensson, and H. Rodhe, 2008: Cloud radiative forcing of subtropical low level clouds in global models. *Climate Dyn.*, **30**, 779–788, https://doi.org/10.1007/s00382-007-0322-1.

Kerr, R. A., 2000: A North Atlantic climate pacemaker for the centuries. *Science*, **288**, 1984–1985, https://doi.org/10.1126/science.288.5473.1984.

Knight, J. R., R. J. Allan, C. K. Folland, M. Vellinga, and M. E. Mann, 2005: A signature of persistent natural thermohaline circulation cycles in observed climate. *Geophys. Res. Lett.*, **32**, L20708, https://doi.org/10.1029/2005GL024233.

——, C. K. Folland, and A. A. Scaife, 2006: Climate impacts of the Atlantic multidecadal oscillation. *Geophys. Res. Lett.*, **33**, L17706, https://doi.org/10.1029/2006GL026242.

Koseki, S., N. Keenlyside, T. Demissie, T. Toniazzo, F. Counillon, I. Bethke, M. Ilicak, and M.-L. Shen, 2018: Causes of the large

warm bias in the Angola-Benguela Frontal Zone in the Norwegian Earth System Model. *Climate Dyn.*, **50**, 4651–4670, https://doi.org/10.1007/s00382-017-3896-2.

Lauer, A., and K. Hamilton, 2013: Simulating clouds with global climate models: A comparison of CMIP5 results with CMIP3 and satellite data. *J. Climate*, **26**, 3823–3845, https://doi.org/10.1175/JCLI-D-12-00451.1.

Li, G., and S.-P. Xie, 2014: Tropical biases in CMIP5 multimodel ensemble: The excessive equatorial Pacific cold tongue and double ITCZ problems. *J. Climate*, **27**, 1765–1780, https://doi.org/10.1175/JCLI-D-13-00337.1.

Lin, J.-L., T. Qian, and T. Shinoda, 2014: Stratocumulus clouds in southeastern Pacific simulated by eight CMIP5–CFMIP global climate models. *J. Climate*, **27**, 3000–3022, https://doi.org/10.1175/JCLI-D-13-00376.1.

Lindzen, R. S., and S. Nigam, 1987: On the role of sea surface temperature gradients in forcing low-level winds and convergence in the tropics. *J. Atmos. Sci.*, **44**, 2418–2436, https://doi.org/10.1175/1520-0469(1987)044<2418:OTROSS>2.0.CO;2.

Liu, W., Z. Liu, J. Cheng, and H. Hu, 2015: On the stability of the Atlantic meridional overturning circulation during the last deglaciation. *Climate Dyn.*, **44**, 1257–1275, https://doi.org/10.1007/s00382-014-2153-1.

Loeb, N. G., and Coauthors, 2018: Clouds and the Earth's Radiant Energy System (CERES) Energy Balanced and Filled (EBAF) top-of-the-atmosphere (TOA) edition 4.0 data product. *J. Climate*, **31**, 895–918, https://doi.org/10.1175/JCLI-D-17-0208.1.

Lu, R., and B. Dong, 2008: Response of the Asian summer monsoon to weakening of Atlantic thermohaline circulation. *Adv. Atmos. Sci.*, **25**, 723–736, https://doi.org/10.1007/s00376-008-0723-z.

Ma, C.-C., C. R. Mechoso, A. W. Robertson, and A. Arakawa, 1996: Peruvian stratus clouds and the tropical Pacific circulation: A coupled ocean–atmosphere GCM study. *J. Climate*, **9**, 1635–1645, https://doi.org/10.1175/1520-0442(1996)009<1635:PSCATT>2.0.CO;2.

McGregor, S., M. F. Stuecker, J. B. Kajtar, M. H. England, and M. Collins, 2018: Model tropical Atlantic biases underpin diminished Pacific decadal variability. *Nat. Climate Change*, **8**, 493–498, https://doi.org/10.1038/s41558-018-0163-4.

Mechoso, C. R., and Coauthors, 1995: The seasonal cycle over the tropical Pacific in coupled ocean–atmosphere general circulation models. *Mon. Wea. Rev.*, **123**, 2825–2838, https://doi.org/10.1175/1520-0493(1995)123<2825:TSCOTT>2.0.CO;2.

——, and Coauthors, 2016: Can reducing the incoming energy flux over the Southern Ocean in a CGCM improve its simulation of tropical climate? *Geophys. Res. Lett.*, **43**, 11 057–11 063, https://doi.org/10.1002/2016GL071150.

Menary, M. B., and A. A. Scaife, 2014: Naturally forced multidecadal variability of the Atlantic meridional overturning circulation. *Climate Dyn.*, **42**, 1347–1362, https://doi.org/10.1007/s00382-013-2028-x.

——, D. L. Hodson, J. I. Robson, R. T. Sutton, R. A. Wood, and J. A. Hunt, 2015: Exploring the impact of CMIP5 model biases on the simulation of North Atlantic decadal variability. *Geophys. Res. Lett.*, **42**, 5926–5934, https://doi.org/10.1002/2015GL064360.

Nnamchi, H. C., J. Li, F. Kucharski, I. S. Kang, N. S. Keenlyside, P. Chang, and R. Farneti, 2015: Thermodynamic controls of the Atlantic Niño. *Nat. Commun.*, **6**, 8895, https://doi.org/10.1038/ncomms9895.

North, G. R., T. L. Bell, R. F. Cahalan, and F. J. Moeng, 1982: Sampling errors in the estimation of empirical orthogonal functions. *Mon. Wea. Rev.*, **110**, 699–706, https://doi.org/10.1175/1520-0493(1982)110<0699:SEITEO>2.0.CO;2.

Oueslati, B., and G. Bellon, 2015: The double ITCZ bias in CMIP5 models: Interaction between SST, large-scale circulation and precipitation. *Climate Dyn.*, **44**, 585–607, https://doi.org/10.1007/s00382-015-2468-6.

Persechino, A., R. Marsh, B. Sinha, A. P. Megann, A. T. Blaker, and A. L. New, 2012: Decadal-timescale changes of the Atlantic overturning circulation and climate in a coupled climate model with a hybrid-coordinate ocean component. *Climate Dyn.*, **39**, 1021–1042, https://doi.org/10.1007/s00382-012-1432-y.

Rayner, N. A., D. E. Parker, E. B. Horton, C. K. Folland, L. V. Alexander, D. P. Rowell, E. C. Kent, and A. Kaplan, 2003: Global analyses of sea surface temperature, sea ice, and night marine air temperature since the late nineteenth century. *J. Geophys. Res.*, **108**, 4407, https://doi.org/10.1029/2002JD002670.

Richter, I., 2015: Climate model biases in the eastern tropical oceans: Causes, impacts and ways forward. *Wiley Interdiscip. Rev.: Climate Change*, **6**, 345–358, https://doi.org/10.1002/wcc.338.

——, and S.-P. Xie, 2008: On the origin of equatorial Atlantic biases in coupled general circulation models. *Climate Dyn.*, **31**, 587–598, https://doi.org/10.1007/s00382-008-0364-z.

——, ——, A. T. Wittenberg, and Y. Masumoto, 2012: Tropical Atlantic biases and their relation to surface wind stress and terrestrial precipitation. *Climate Dyn.*, **38**, 985–1001, https://doi.org/10.1007/s00382-011-1038-9.

——, ——, S. K. Behera, T. Doi, and Y. Masumoto, 2014: Equatorial Atlantic variability and its relation to mean state biases in CMIP5. *Climate Dyn.*, **42**, 171–188, https://doi.org/10.1007/s00382-012-1624-5.

Rodriguez-Fonseca, B., I. Polo, J. García-Serrano, T. Losada, E. Mohino, C. R. Mechoso, and F. Kucharski, 2009: Are Atlantic Niños enhancing Pacific ENSO events in recent decades? *Geophys. Res. Lett.*, **36**, L20705, https://doi.org/10.1029/2009GL040048.

Ruprich-Robert, Y., R. Msadek, F. Castruccio, S. Yeager, T. Delworth, and G. Danabasoglu, 2017: Assessing the climate impacts of the observed Atlantic multidecadal variability using the GFDL CM2.1 and NCAR CESM1 global coupled models. *J. Climate*, **30**, 2785–2810, https://doi.org/10.1175/JCLI-D-16-0127.1.

Sasaki, W., T. Doi, K. J. Richards, and Y. Masumoto, 2014: Impact of the equatorial Atlantic sea surface temperature on the tropical Pacific in a CGCM. *Climate Dyn.*, **43**, 2539–2552, https://doi.org/10.1007/s00382-014-2072-1.

Shi, Y., W. Huang, B. Wang, Z. Yang, X. He, and T. Qiu, 2018: Origin of warm SST bias over the Atlantic cold tongue in the coupled climate model FGOALS-g2. *Atmosphere*, **9**, 275, https://doi.org/10.3390/atmos9070275.

Shu, Q., Z. Song, and F. Qiao, 2015: Assessment of sea ice simulations in the CMIP5 models. *Cryosphere*, **9**, 399–409, https://doi.org/10.5194/tc-9-399-2015.

Song, Z., S.-K. Lee, C. Wang, B. P. Kirtman, and F. Qiao, 2015: Contributions of the atmosphere–land and ocean–sea ice model components to the tropical Atlantic SST bias in CESM1. *Ocean Modell.*, **96**, 280–290, https://doi.org/10.1016/j.ocemod.2015.09.008.

Stubenrauch, C. J., and Coauthors, 2013: Assessment of global cloud datasets from satellites; Project and database initiated by the GEWEX Radiation Panel. *Bull. Amer. Meteor. Soc.*, **94**, 1031–1049, https://doi.org/10.1175/BAMS-D-12-00117.1.

Takatama, K., S. Minobe, M. Inatsu, and R. J. Small, 2012: Diagnostics for near- surface wind convergence/divergence re-

sponse to the Gulf Stream in a regional atmospheric model. *Atmos. Sci. Lett.*, **13**, 16–21, https://doi.org/10.1002/asl.355.

Taylor, K. E., R. J. Stouffer, and G. A. Meehl, 2012: An overview of CMIP5 and the experiment design. *Bull. Amer. Meteor. Soc.*, **93**, 485–498, https://doi.org/10.1175/BAMS-D-11-00094.1.

Timmermann, A., and Coauthors, 2007: The influence of a weakening of the Atlantic meridional overturning circulation on ENSO. *J. Climate*, **20**, 4899–4919, https://doi.org/10.1175/JCLI4283.1.

Ting, M., Y. Kushnir, R. Seager, and C. Li, 2009: Forced and internal twentieth-century SST trends in the North Atlantic. *J. Climate*, **22**, 1469–1481, https://doi.org/10.1175/2008JCLI2561.1.

——, ——, ——, and ——, 2011: Robust features of Atlantic multidecadal variability and its climate impacts. *Geophys. Res. Lett.*, **38**, L17705, https://doi.org/10.1029/2011GL048712.

Toniazzo, T., and S. Woolnough, 2014: Development of warm SST errors in the southern tropical Atlantic in CMIP5 decadal hindcasts. *Climate Dyn.*, **43**, 2889–2913, https://doi.org/10.1007/s00382-013-1691-2.

Turner, J., T. J. Bracegirdle, T. Phillips, G. J. Marshall, and J. S. Hosking, 2013: An initial assessment of Antarctic sea ice extent in the CMIP5 models. *J. Climate*, **26**, 1473–1484, https://doi.org/10.1175/JCLI-D-12-00068.1.

Voldoire, A., M. Claudon, G. Caniaux, H. Giordani, and R. Roehrig, 2014: Are atmospheric biases responsible for the tropical Atlantic SST biases in the CNRM-CM5 coupled model? *Climate Dyn.*, **43**, 2963–2984, https://doi.org/10.1007/s00382-013-2036-x.

von Storch, H., and F. W. Zwiers, 2003: *Statistical Analysis in Climate Research*. Cambridge University Press, 484 pp.

Wang, C., L. Zhang, S. K. Lee, L. Wu, and C. R. Mechoso, 2014: A global perspective on CMIP5 climate model biases. *Nat. Climate Change*, **4**, 201–205, https://doi.org/10.1038/nclimate2118.

Wu, L., C. Li, C. Yang, and S. P. Xie, 2008: Global teleconnections in response to a shutdown of the Atlantic meridional overturning circulation. *J. Climate*, **21**, 3002–3019, https://doi.org/10.1175/2007JCLI1858.1.

Xiang, B., M. Zhao, I. M. Held, and J. C. Golaz, 2017: Predicting the severity of spurious "double ITCZ" problem in CMIP5 coupled models from AMIP simulations. *Geophys. Res. Lett.*, **44**, 1520–1527, https://doi.org/10.1002/2016GL071992.

Xu, Z., P. Chang, I. Richter, and G. Tang, 2014: Diagnosing southeast tropical Atlantic SST and ocean circulation biases in the CMIP5 ensemble. *Climate Dyn.*, **43**, 3123–3145, https://doi.org/10.1007/s00382-014-2247-9.

Zermeño-Diaz, D. M., and C. Zhang, 2013: Possible root causes of surface westerly biases over the equatorial Atlantic in global climate models. *J. Climate*, **26**, 8154–8168, https://doi.org/10.1175/JCLI-D-12-00226.1.

Zhang, L., and C. Wang, 2013: Multidecadal North Atlantic sea surface temperature and Atlantic meridional overturning circulation variability in CMIP5 historical simulations. *J. Geophys. Res. Oceans*, **118**, 5772–5791, https://doi.org/10.1002/jgrc.20390.

——, ——, Z. Song, and S. K. Lee, 2014: Remote effect of the model cold bias in the tropical North Atlantic on the warm bias in the tropical southeastern Pacific. *J. Adv. Model. Earth Syst.*, **6**, 1016–1026, https://doi.org/10.1002/2014MS000338.

Zhang, R., 2007: Anticorrelated multidecadal variations between surface and subsurface tropical North Atlantic. *Geophys. Res. Lett.*, **34**, L12713, https://doi.org/10.1029/2007GL030225.

Zhu, C., Z. Liu, and S. Gu, 2018: Model bias for South Atlantic Antarctic intermediate water in CMIP5. *Climate Dyn.*, **50**, 3613–3624, https://doi.org/10.1007/s00382-017-3828-1.

Zuidema, P., and Coauthors, 2016: Challenges and prospects for reducing coupled climate model SST biases in the eastern tropical Atlantic and Pacific Oceans: The U.S. CLIVAR Eastern Tropical Oceans Synthesis Working Group. *Bull. Amer. Meteor. Soc.*, **97**, 2305–2328, https://doi.org/10.1175/BAMS-D-15-00274.1.